# INCORPORATION OF A GENERAL STRAIN-TO-FAILURE FRACTURE CRITERION INTO A STRESS-BASED PLASTICITY MODEL THROUGH A TIME-TO-FAILURE SOFTENING MECHANISM

by

Matthew Scot Swan

A thesis submitted to the faculty of
The University of Utah
in partial fulfillment of the requirements for the degree of

Master of Science

Department of Mechanical Engineering

The University of Utah

May 2012

**The University of Utah Graduate School**

# STATEMENT OF THESIS APPROVAL

The thesis of **Matthew Scot Swan**

has been approved by the following supervisory committee members:

| | | |
|---|---|---|
| **Rebecca M. Brannon** | , Chair | **12 Jan 2012** Date Approved |
| **K. Larry DeVries** | , Member | **12 Jan 2012** Date Approved |
| **K.S. Ravi Chandran** | , Member | **12 Jan 2012** Date Approved |

and by **Timothy A. Ameel** , Chair of the Department of **Mechanical Engineering**

and by Charles A. Wight, Dean of The Graduate School.

# ABSTRACT

Many classic and contemporary fracture models are based on some variant of strain-to-failure with linear accumulation of damage. These models are categorized as strain-to-failure models, even if the damage weighting function is stress-based. Recent experimental investigations suggest that strain-to-failure fracture models are a natural choice when modeling metals. Notably, the third stress invariant ($J_3$) dependence of strain-to-failure has been shown to be nonnegligible. In response to the metal-fracture literature proposing a multitude of new strain-to-failure fracture models with little demonstration of predictiveness in large-scale general-loading simulations, this research implements a strain-to-failure framework into a generalized plasticity model, Kayenta, tested in conjunction with three representative fracture models: constant equivalent-strain-to-failure, Johnson-Cook strain-to-failure theory, and Xue-Wierzbicki strain-to-failure theory. These models constitute a sampling of $J_2$, $J_3$, strain-rate, and temperature dependence that greatly extend the softening options available in Kayenta. As Kayenta is portable and already available in multiple host codes, this research allows analysts to rapidly gauge which failure theory is best suited to their applications, thus potentially allowing one of these theories to emerge as more broadly valid in general loading problems. This fracture framework is designed to operate in the realm of time-to-failure so as to function seamlessly with the current softening implementation in Kayenta and lay the foundation for mixed-response fracture behavior to transition between ductile to brittle fracture models dynamically as the stress state evolves.

# CONTENTS

# LIST OF FIGURES

# LIST OF TABLES

# ACKNOWLEDGMENTS

I would especially like to thank my advisor, Professor Rebecca Brannon, for her guidance throughout my undergraduate and graduate careers; her wisdom and insight have greatly expanded my view of the field of computational solid mechanics, math, and science in general.

I am also grateful to my fellow students and colleagues for their help and assistance. Specifically, I would like to thank Krishna Kamojjala for his help in running the validation simulations and being the beta user for the newly-implemented fracture models. Both Michael Homel and Seubpong Leelavanichkul have been invaluable in proofreading and critiquing my thesis.

I have been the recipient of much help from my colleagues at Sandia National Laboratories. My manager and mentor, Erik Strack, has been a pivotal figure in my professional development. He has shown me great kindness and has been an excellent example; simply put, he is the best. Mike Wong, Joseph Bishop, and Tim Fuller have all instructed me and worked with me to expand my knowledge of damage models in general as well as enabling me to make lasting contributions to Kayenta. I would also like to recognize Idaho National Laboratory for formulation of the unnotched Charpy impact problem used as validation of the framework implementation.

This work was partially funded by a Sandia National Laboratories Laboratory Directed Research and Development (LDRD) project and is gratefully acknowledged.

Finally, I want to thank my wife for her help, support, patience, and love.

Sandia National Laboratories is a multi-program laboratory managed and operated by Sandia Corporation, a wholly owned subsidiary of Lockheed Martin Corporation, for the U.S. Department of Energys National Nuclear Security Administration under contract DE-AC04-94AL85000.


# CHAPTER 1

# INTRODUCTION

Material fracture is difficult to predict in numerical modeling of materials. The fracture pattern and response are heavily dependent on mesh geometry [5], model choice [6], and evolution laws (*e.g.,* hardening) [7]. Taking these into consideration, it is convenient to have a generalized plasticity model with the ability to reproduce strain-to-failure behavior for the large class of damage models that are based on linear accumulation of damage. Strain-to-failure models assume that fracture is predictable as a function of strain for a given loading path. These models have been in use for decades and give acceptable results for simple, isothermal loading [4]. This research is aimed at allowing rapid prototyping and evaluation of fracture models by incorporating a variety of fracture options into Kayenta, a unified general-purpose plasticity model which is already adopted by researchers across the nation and overseas. By being able to mimic many different classical theories in a unified framework, a general-purpose plasticity model (with support for fracture) allows analysts to explore a variety of constitutive model features to determine those that are most essential to a particular application. The existing modularity that allows Kayenta to function as a multipurpose plasticity model will facilitate broad application and future development of this work.

## 1.1 Motivation

Predictive fracture modeling has many practical applications for industry. The aerospace, automotive, and defense industries generally deal with different materials and different failure mechanisms that can span failure of ductile materials under quasistatic, monotonic loading, brittle metal fracture subject to cyclic loading, and ceramic fracture under impact loading.

Failure modes can vary across materials. For decades, researchers have sought after a model that can give results for tension, compression, shear, low strain rate, high strain rate, and/or varying temperatures with an acceptable accuracy for a given engineering appli-

cation. While a model that covers all loading scenarios perfectly has not been developed, there are a multitude of models that are predictive when applied to a specific material and/or situation.

Accordingly, this research aims to implement recently published cutting-edge fracture models [8, 9] into the hands of researchers and analysts so the models may be exercised and evaluated based on performance in large-scale, real-world problems. The scope of this work is limited to the development of the fracture framework and the implementation and verification of three models into Kayenta, the constant equivalent-strain-to-failure model, the Johnson-Cook fracture model, and the Xue-Wierzbicki fracture model. These models will then be compared against laboratory tests to assess whether the implemented models demonstrate an improvement in predictability over the native Kayenta fracture criterion.

While beyond the scope of the present research, a future possible research direction would be to incorporate an interpolation approximation between failure models based on strain rate. While this has not been investigated, it is reasonable to propose a system of dynamically varying fracture models for different loading conditions to leverage models that are better suited for a particular material state.

## 1.2 Objectives

The present research focuses on the following areas and objectives:

- Perform an in-depth review of current literature concerning strain-to-failure fracture models. Special attention is given to models developed under Tomasz Wierzbicki at the Massachusetts Institute of Technology.
- Create a framework capable of handling strain-to-failure damage models that can be implemented into the generalized plasticity model Kayenta without disrupting the original softening framework.
- Implement into the aforementioned framework three representative fracture models: the constant equivalent-strain-at-failure (CESF) fracture model, the Johnson-Cook (JC) fracture model [3], and the Xue-Wierzbicki (XW) fracture model [4]. These models were chosen to demonstrate varying levels of stress dependence in fracture prediction.
- Perform extensive verification of the framework and exercise the three models for varying load conditions.
- Apply the new fracture models to a validation problem that exercises the models and framework in a real-world application.
- Identify directions for future work that could extend this research.

# CHAPTER 2

# DEFINITIONS AND TERMINOLOGY

Throughout this document, a consistent notation will be used to differentiate between scalars, vectors, and tensors. For clarity, the under-tilde will be adopted to explicitly state the order of the tensor. As a scalar is a zero-order tensor, no under-tilde is provided. A vector is a first-order tensor and will have one. The usual second-order tensor will have two. For example:

$$\begin{array}{l} \text{scalar (zeroth-order): } \eta \\ \text{vector (first-order): } \underset{\sim}{\boldsymbol{v}} \\ \text{tensor (second-order): } \underset{\approx}{\boldsymbol{\sigma}} \end{array} \tag{2.1}$$

The underline $\underline{\eta}$ will be used to define "equivalent" scalar values of tensor quantities (individually defined later). The over-bar $\bar{\eta}$ will be used to denote a sign change such that $\bar{\eta} = -\eta$.

## 2.1 The Stress Tensor

The stress tensor is a real-valued, second-order, symmetric tensor [10] with the sign convention that tension corresponds to a positive stress. With respect to the orthonormal "laboratory" basis, the stress tensor's component matrix may be written:

$$[\underset{\approx}{\boldsymbol{\sigma}}] = \begin{bmatrix} \sigma_{11} & \sigma_{12} & \sigma_{13} \\ \sigma_{12} & \sigma_{22} & \sigma_{23} \\ \sigma_{13} & \sigma_{23} & \sigma_{33} \end{bmatrix} \tag{2.2}$$

Recognizing that the stress tensor is real and symmetric, we can apply the spectral theorem [11] to assert existence of an alternative basis (the stress eigenvectors) such that the component matrix may be written in terms of the eigenvalues or principal stresses, $\{\sigma_1, \sigma_2, \sigma_3\}$ as

$$[\underset{\approx}{\boldsymbol{\sigma}}] = \begin{bmatrix} \sigma_1 & 0 & 0 \\ 0 & \sigma_2 & 0 \\ 0 & 0 & \sigma_3 \end{bmatrix} \tag{2.3}$$

For many applications, it is easier to work with this diagonal principal stress matrix than with the fully-populated stress matrix. The principal stresses can be used in vector notation to define a point in 3D Cartesian stress space, called the Haigh-Westergaard space.

The deviatoric part of the stress tensor or the stress deviator, $\underset{\approx}{\boldsymbol{S}}$, is defined as

$$\underset{\approx}{\boldsymbol{S}} = \underset{\approx}{\boldsymbol{\sigma}} - \frac{1}{3}\,\mathrm{tr}(\underset{\approx}{\boldsymbol{\sigma}})\underset{\approx}{\boldsymbol{I}} \tag{2.4}$$

with $\underset{\approx}{\boldsymbol{I}}$ being the identity tensor. By construction, the stress deviator (which is a generalized measure of shear stress) has a zero trace.

## 2.2 Stress Invariant Triplets

Real symmetric tensors in ordinary 3D space have up to three independent invariants. For example, all stress invariants are expressible in terms of the principal stresses, $\{\sigma_1, \sigma_2, \sigma_3\}$. These stress eigenvalues may be viewed as being Cartesian components for the 3D subspace spanned by the eigenprojectors of the stress tensor. The subsections below define commonly-used alternative stress invariant triplets. Changing from one invariant triplet to another is tantamount to making a coordinate change in principal stress space.

### 2.2.1 Principal Invariant Triplet $\{I_1, I_2, I_3\}$

For a symmetric real-valued tensor (in our case, the stress tensor $\underset{\approx}{\boldsymbol{\sigma}}$), the principal invariants [10] are

$$\begin{aligned} I_1 &= \mathrm{tr}(\underset{\approx}{\boldsymbol{\sigma}}) \\ I_2 &= \tfrac{1}{2}\left[\Big(\mathrm{tr}(\underset{\approx}{\boldsymbol{\sigma}})\Big)^2 - \mathrm{tr}(\underset{\approx}{\boldsymbol{\sigma}}^2)\right] \\ I_3 &= \det(\underset{\approx}{\boldsymbol{\sigma}}) \end{aligned} \tag{2.5}$$

These constitute an alternative invariant triplet to the principal stress invariant triplet. If the principal stresses are known, then these principal invariants may be found by substituting Eq.2.3 into 2.5. Conversely, if values of the principal invariants are known, then the eigenvalues are found by solving the characteristic equation, $\sigma^3 - I_1\sigma^2 + I_2\sigma - I_3 = 0$. Thus, having one invariant triplet is sufficient to obtain the other triplet.

### 2.2.2 Mechanics Invariant Triplet, $\{I_1, J_2, J_3\}$

The principal invariants of the stress deviator are $\{J_1, -J_2, J_3\}$, where

$$\begin{aligned} J_1 &= \mathrm{tr}(\underset{\approx}{\boldsymbol{S}}) = 0 \\ J_2 &= -\tfrac{1}{2}\left[\Big(\mathrm{tr}(\underset{\approx}{\boldsymbol{S}})\Big)^2 - \mathrm{tr}(\underset{\approx}{\boldsymbol{S}}^2)\right] = \tfrac{1}{2}\,\mathrm{tr}(\underset{\approx}{\boldsymbol{S}}^2) \\ J_3 &= \det(\underset{\approx}{\boldsymbol{S}}) = \tfrac{1}{3}\,\mathrm{tr}(\underset{\approx}{\boldsymbol{S}}^3) \end{aligned} \tag{2.6}$$

The negative sign is introduced in the definition of $J_2$ to ensure that it will always be positive. In fact, $J_2 = \frac{1}{\sqrt{2}}||\underset{\approx}{\boldsymbol{S}}||$. Since $J_1 = 0$, the set $\{J_1, J_2, J_3\}$ cannot be regarded as an independent invariant triplet. Specifically, having values for $\{J_1, J_2, J_3\}$ is insufficient to

determine the value of $I_1$. For this reason, the so-called "mechanics invariants" [1] are an independent invariant triplet defined by $\{I_1, J_2, J_3\}$.

### 2.2.3 Lode Coordinate Invariant Triplet, $\{r, \theta, z\}$

From the previous set of three independent tensor invariants we can define another, geometrically intuitive, set of three invariants called the Lode invariants. The Lode invariants may be regarded as cylindrical coordinates for principal stress space as an alternative to the Cartesian coordinates given by the principal stresses. The name is derived from W. Lode, a German Engineer, who is first attributed with use of the Lode angle in 1926 [12].

Lode coordinates, in terms of the mechanics invariants of the stress tensor, are defined by

$$z = \frac{I_1}{\sqrt{3}} \tag{2.7}$$

$$r = \sqrt{2J_2} \tag{2.8}$$

$$\theta = \frac{1}{3}\sin^{-1}\left(\frac{J_3}{2}\left(\frac{3}{J_2}\right)^{3/2}\right) \tag{2.9}$$

and form a set of cylindrical coordinates centered about the hydrostat (i.e., the set of all isotropic stress states).

The coordinate $z$ is a constant multiple of pressure $p = -\frac{1}{3}I_1$, and $r$ is a constant multiple of equivalent shear stress $\tau^{\text{eq}} = \sqrt{J_2}$. Because of these multiples, a plot of $r$ vs. $z$ (called a meridional view) is isomorphic to the 2D subspace spanned by the stress deviator and the identity tensor. Lacking such multiples, a more conventional plot of $\tau^{\text{eq}}$ vs. $p$ is actually a geometrically distorted (and hence potentially misleading) view of stress space.

The Lode angle $\theta$ varies monotonically with the position of the middle principal stress relative to the high and low principal stresses. Specifically, as the middle eigenvalue moves from the left side to the right side of the outer Mohr's circle in a Mohr diagram, the Lode angle will vary linearly from $\pi/6$ to $-\pi/6$ (see Fig. 2.1). When $r = 0$, the Lode angle is mathematically undefined, but is here assumed that $\theta = 0$ in such situations.

### 2.2.4 Fracture Invariant Triplet, $\{\sigma_m, \eta, \xi\}$

Two commonly-used scalar stress measures are the mean stress and the von Mises equivalent stress, defined in terms of the principal stresses respectively by

$$\sigma_m = \frac{I_1}{3} = \frac{\sigma_1 + \sigma_2 + \sigma_3}{3} \tag{2.10}$$

$$\underline{\sigma} = \sqrt{3J_2} = \sqrt{\frac{(\sigma_1 - \sigma_2)^2 + (\sigma_2 - \sigma_3)^2 + (\sigma_3 - \sigma_1)^2}{2}} \tag{2.11}$$

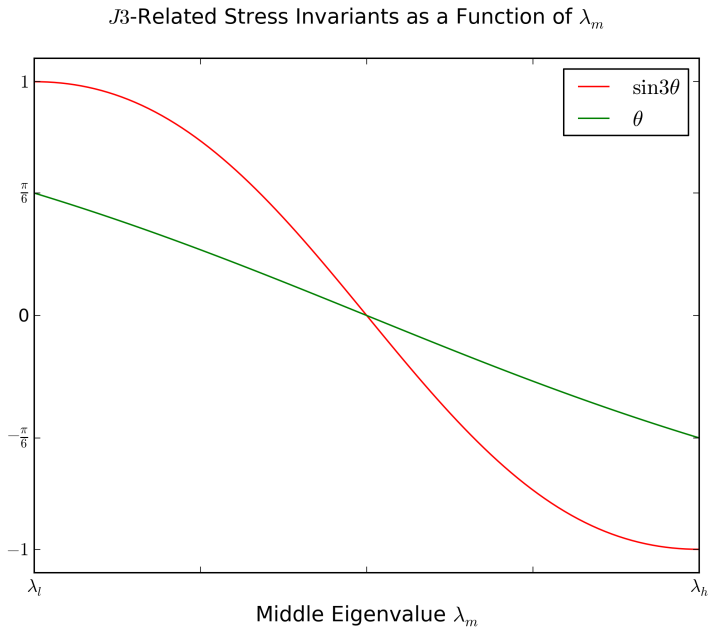


**Figure 2.1**: Depiction of $\theta$ and $\xi$ ($\sin 3\theta$) as a function of the placement of the middle eigenvalue $\lambda_m$ in relation to the low and high eigenvalues, $\lambda_l$ and $\lambda_h$, respectively.

The fracture literature often refers to a dimensionless pressure-stress ratio, called stress triaxiality, $\eta$, defined by [13]

$$\eta = \frac{\sigma_m}{\underline{\sigma}} = \frac{I_1}{3\sqrt{3J_2}} \tag{2.12}$$

This equation corresponds to a positive infinite value for hydrostatic tension, a negative infinite value for hydrostatic compression, and a zero value for pure shear.

It is also common to see the deviatoric state parameter or Lode parameter $\xi$ in the fracture literature. It is defined much like the Lode angle $\theta$ and varies over the range $[-1, 1]$ [13]

$$\xi = \frac{J_3}{2}\left(\frac{3}{J_2}\right)^{3/2} = \sin 3\theta \tag{2.13}$$

The second two fracture invariants are homogeneous of degree zero with respect to stress, meaning that knowing the ratio of the stresses is sufficient to calculate their values. Because of this fact, we can compute values for $\eta$ and $\xi$ without stress magnitude. Table 2.1 contains values for common stress states. It is straightforward to demonstrate that $\{\sigma_m, \eta, \xi\}$ constitute an admissible alternative invariant triplet for stress space in the sense that having values for this triplet is sufficient to find values of any other invariant.

## 2.3 Strain Measures

Strain measures are many and varied, with different definitions being employed occasionally under the same title. To alleviate this difficulty, this discussion will focus on

**Table 2.1**: A comparison of the fracture invariants $\eta$ (stress triaxiality) and $\xi$ (deviatoric state parameter/Lode parameter) for common loading conditions. These two fracture invariants are homogeneous of degree zero with respect to stress, meaning that knowing the ratio of stresses is sufficient to calculate their values.

| Fracture Invariants for Common Stress States | | |
|---|---|---|
| Stress State | $\eta$ | $\xi$ |
| Hydrostatic Tension | $\infty$ | undef |
| Biaxial Tension | $2/3$ | $-1$ |
| Uniaxial Tension | $1/3$ | $+1$ |
| Shear | $0$ | $0$ |
| Uniaxial Compression | $-1/3$ | $-1$ |
| Biaxial Compression | $-2/3$ | $+1$ |
| Hydrostatic Compression | $-\infty$ | undef |

defining a strain tensor from the deformation gradient tensor, $\underset{\approx}{\boldsymbol{F}}$. As strain contains no information about rotation, our strain definition will apply the polar decomposition theorem to extract the right Cauchy stretch tensor, $\underset{\approx}{\boldsymbol{U}}$, as described in any modern Continuum Mechanics textbook (cf., [10]).

### 2.3.1 Strain Tensor

Restating the conclusion of Seth [14], a whole family of strain tensors can be defined from the stretch tensor for different integer values of $\kappa$ by

$$\underset{\approx}{\boldsymbol{\varepsilon}} = \frac{1}{\kappa}\left(\underset{\approx}{\boldsymbol{U}}^{\kappa} - \underset{\approx}{\boldsymbol{I}}\right) \tag{2.14}$$

When $\kappa = 0$, the limit form of this equation must be used. Table 2.2 contains common names associated with the strain measure for common values of $\kappa$. Future references to strain, in scalar or tensor form, should be assumed to refer to the logarithmic strain ($\kappa = 0$) form of that strain measure unless otherwise stated.

**Table 2.2**: Sampling of names encountered in the literature for common strain measures in the Seth-Hill family of strains for integer values of $\kappa$.

| Common Strain Names | |
|---|---|
| $\kappa$ | Name(s) |
| $-2$ | Green |
| $-1$ | True, Cauchy |
| $0$ | Logarithmic, Hencky, True |
| $1$ | Engineering, Swainger |
| $2$ | Lagrange, Almansi |

### 2.3.2 Equivalent Strain

Much like the von Mises equivalent stress, equivalent strain is a measure of the deviatoric part of the elastic, plastic, or total strain tensor. In this research, only the equivalent plastic strain will be discussed. It is defined by

$$\underline{\varepsilon}^p = \sqrt{\frac{2}{3}\,\mathrm{tr}\left(\mathrm{dev}(\underset{\approx}{\boldsymbol{\varepsilon}^{\boldsymbol{p}}}) \cdot \mathrm{dev}(\underset{\approx}{\boldsymbol{\varepsilon}^{\boldsymbol{p}}})\right)} \tag{2.15}$$

where $\underset{\approx}{\boldsymbol{\varepsilon}^{\boldsymbol{p}}}$ is the plastic part of the strain tensor.

## 2.4 Classical Kayenta Softening

### 2.4.1 Damage and Coherence

The term "coherence" (the state variable `COHER` in Kayenta [1]) is a process parameter that varies from 1 for a virgin material to 0 for a material that is regarded as having lost as much strength as it is possible to lose. Being merely a process parameter, coherence lacks physical meaning until it is used to parameterize the evolution of physical variables such as the shear strength. We will herein refer to coherence strictly as a variable that represents the evolution of a material as it tends towards loss of stiffness and strength as result of fracture (e.g., we do not consider other physical mechanics, such as melting, that can likewise reduce stiffness or strength).

When modeling deformation up to fracture, many theories [3, 9] define a damage evolution law that permits the damage parameter (which is separate from coherence) to increase without any loss of strength or stiffness until damage reaches a value of unity. In this research, the damage (or fracture) models simply dictate when the material fails and allow the built-in softening mechanism of Kayenta to handle the loss of strength and degradation of elastic moduli through decreasing coherence.

The damage parameter is defined over the interval $[0, 1]$, with 0 corresponding to perfectly undamaged, intact material and 1 corresponding to failed, fractured material. For convenience, damage is herein constrained to be a monotonically increasing value, but there are no constraints in the framework that would impede permitting damage to both increase and decrease (which is called material healing).

The coherence parameter is much like damage in that it is defined over the interval $[0, 1]$. However, the fully intact element has a coherence value of 1 while a fully fractured, softened element with degraded strength has a coherence value of 0. Coherence is constrained to be a monotonically decreasing value, also imposed by the assumption of no material healing.

Engineering plasticity and damage models typically employ two types of surfaces, the yield surface (which is the boundary of elastically obtainable stress states) and the limit

surface (which is the boundary of stress states attainable by any means, elastic or plastic). Examples of these surfaces are illustrated in Fig. 2.2. By definition, a yield surface must be contained entirely within the limit surface, and a yield surface can evolve by expanding outward (isotropic hardening) or translating (kinematic hardening) towards the limit surface to allow the stress state to move from the initial elastic limit value to a peak value on the limit surface. If the yield surface cannot evolve, then the yield surface and the limit surface are equal. When softening occurs, the limit surface collapses and forces the yield surface to partially or fully collapse because the yield surface must reside within the limit surface. A depiction of a limit surface collapse is shown in Fig. 2.3.

As illustrated in Fig. 2.4, reaching the limit surface corresponds to achieving a peak

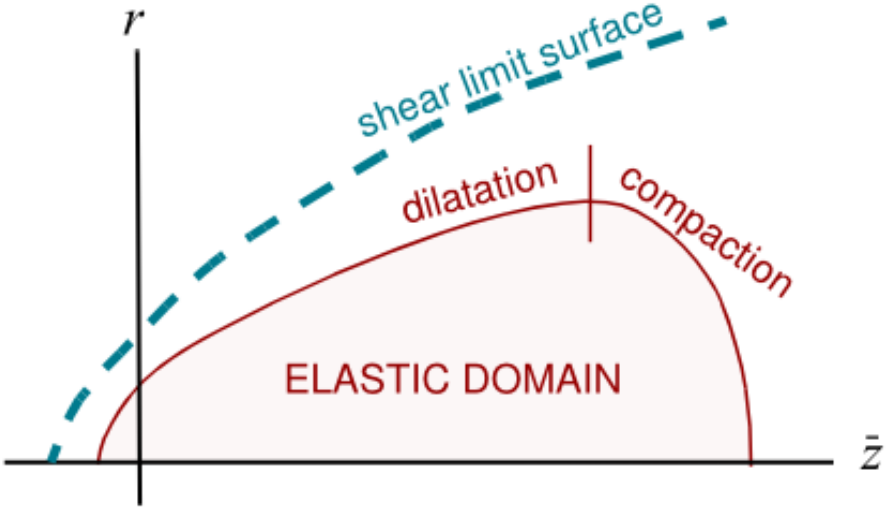


**Figure 2.2**: Depiction of a possible initial yield surface (boundary of the elastically attainable stress states) and limit surface. This research focuses on the shape and placement of the limit surface and its collapse when fracture occurs. Reproduced with permission [1].

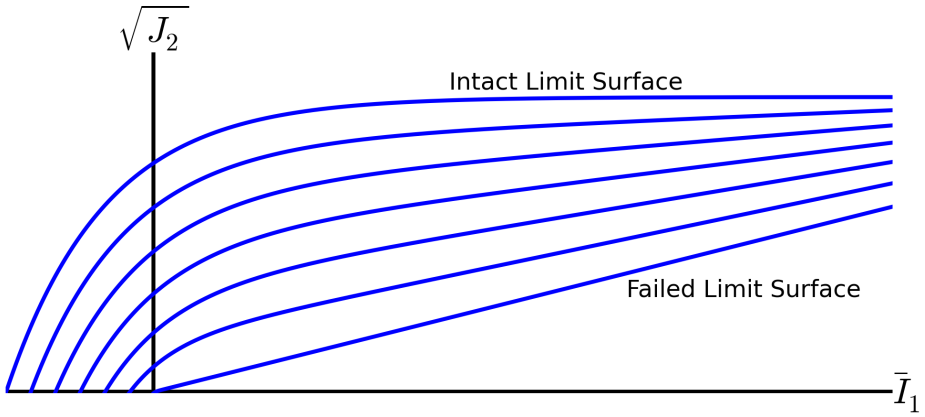


**Figure 2.3**: Stages of a possible limit surface collapse after damage reaches unity.

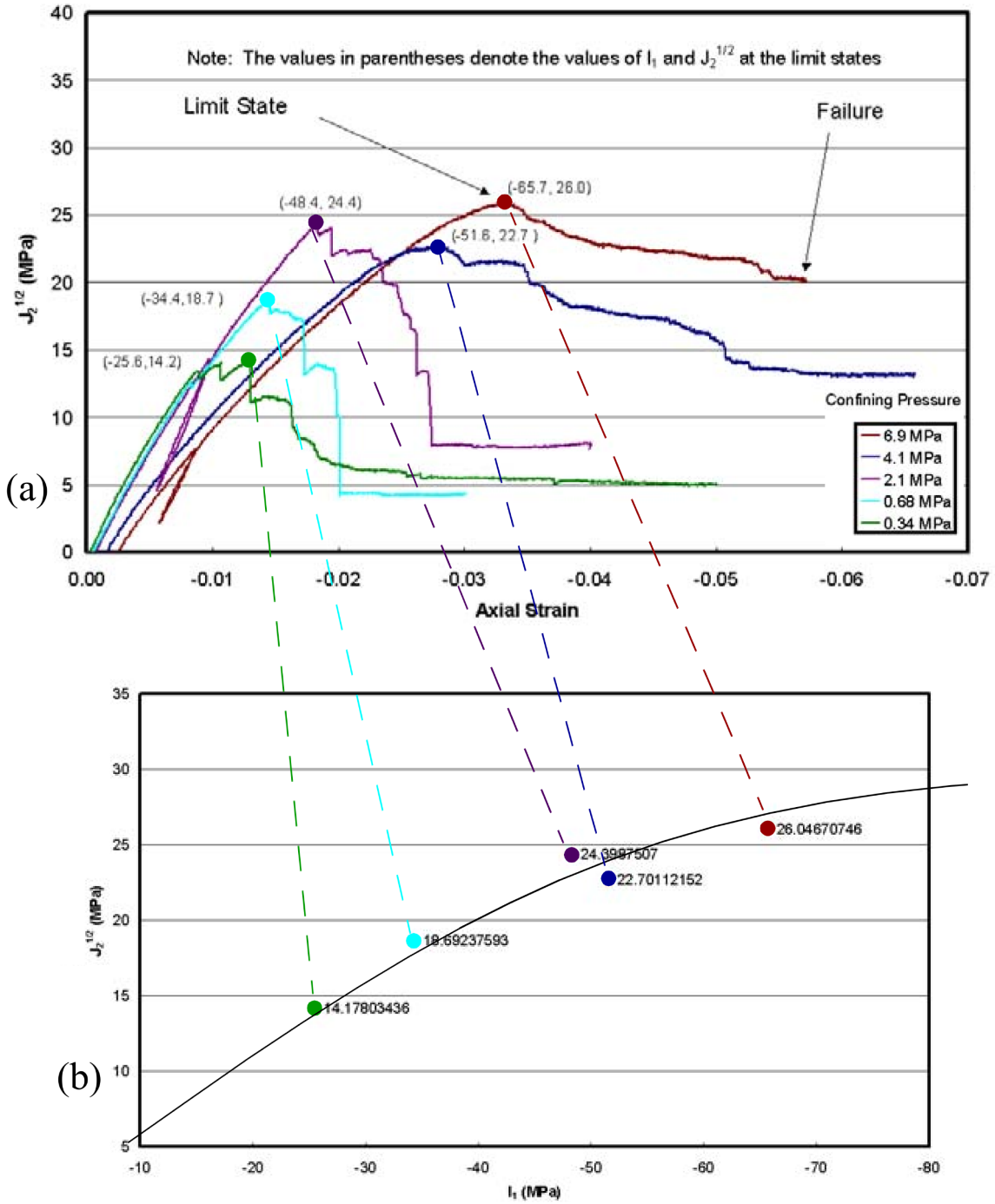


**Figure 2.4**: Example of the relationship between the limit surface and postpeak softening. (a) Experimental data showing peak stresses at the limit surface followed by softening. (b) Conversion of these experimental data to determine the form of the limit surface. Reproduced with permission [1].

stress value in a measured stress-strain curve, after which the material loses strength and fails catastrophically at a much lower stress and much higher strain than the stress and strain values at the peak state. The degradation of the stress from the peak strength to the ultimate strength is accommodated in Kayenta by collapse of the limit surface. However, this is implemented without any validated evolution equations governing the rate of limit surface collapse. This implementation is intended to capture the experimental trend of the loss of strength during the transition from the peak strength to the ultimate failure state (i.e., the region of a stress-strain curve having negative slope).

### 2.4.2 TGROW and TFAIL

In the classical Kayenta softening routines, coherence is tracked while damage is not. In the place of damage there are two values called TGROW and TFAIL. The variable TGROW is a timer that tracks the total time that the stress state has been at the limit surface and TFAIL is a material-specific characteristic failure time for a given loading condition and element size. When TGROW and TFAIL are approximately equal, material softening occurs. Specifically, coherence drops most rapidly when TGROW = TFAIL.

As seen in Fig. 2.5, coherence can drop somewhat prior to TGROW reaching TFAIL, and coherence can likewise continue to evolve at a moderate rate for TGROW > TFAIL. As illustrated, a control parameter called FSPEED is available to control the rate of change of coherence with respect to the ratio of TGROW to TFAIL. Large values of FSPEED imply a sudden drop of coherence at TGROW = TFAIL, whereas small values of FSPEED allow a more gradual drop.

TGROW is a monotonic state variable that can increase only when the stress state is on the limit surface. The rate of TGROW is not constant and is determined by the angle made by the trial stress increment with the normal to the yield surface. When these two are parallel, the time rate of TGROW is unity, whereas when the two directions are mutually orthogonal, the time rate of TGROW is zero. This implies that a stress trajectory that reaches the yield surface and begins to circumscribe the yield surface will maintain a constant TGROW time rate of zero, thus never losing strength as TGROW cannot approach TFAIL. This implementation of softening does not allow for fracture to occur unless the material stress state has attained the limit surface. This could allow for nonrealistic predictions where no fracture occurs solely because the stress state never attained the limit surface.

The evolution of COHER is a simple function of TGROW/TFAIL and is defined by

$$\texttt{COHER} = \frac{1 + e^{-2\texttt{FSPEED}}}{1 + e^{-2\texttt{FSPEED}(1-\texttt{TGROW}/\texttt{TFAIL})}} \tag{2.16}$$

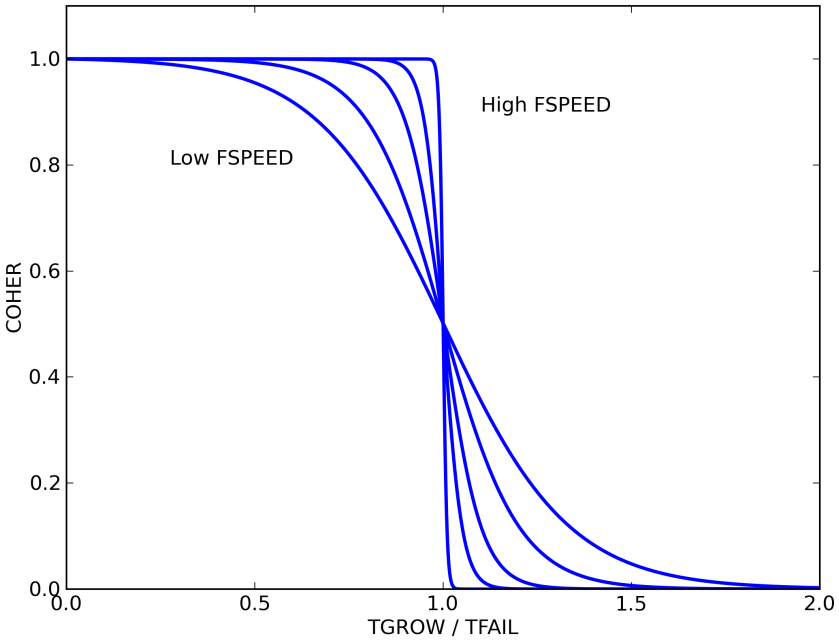


**Figure 2.5**: Evolution of coherence as `TGROW` increases with respect to `TFAIL`.

While `TGROW` $\ll$ `TFAIL` or `TGROW` $\gg$ `TFAIL`, there is essentially no change in `COHER` for changes in `TGROW` or `TFAIL`. However, when `TGROW` $\approx$ `TFAIL` small changes in either will cause a change to occur in `COHER`. As mentioned above, it is expected that the values of `COHER` will monotonically decrease with respect to simulation time. The value of `COHER` might drop in one timestep then, due to changing loading conditions, the following time step would compute a higher value of `COHER`. Because of this, `COHER` is not permitted to increase from time step to time step.

# CHAPTER 3

# LITERATURE REVIEW

## 3.1 Common Fracture Models

Among fracture models in use today, the simple constant equivalent-strain-to-failure (CESF) model is most prevalent in widely-used commercial and open-source codes [15, 16]. It is also commonly used as a benchmark for comparing other fracture models [4, 17].

While the CESF model is easy to use and to parameterize [4], it has been found to be nonpredictive for stress states that are not similar to the calibration experiment [17]. A generalized model for varied loading paths should incorporate dependence on stress triaxiality (which depends on the stress invariants $I_1$ and $J_2$), as it has been found to be the most important factor in inelastic material evolution [18, 19].

In 1980, M.L. Wilkins published a paper [20] describing a cumulative strain-to-failure damage model with $J_2$ dependence. Building on that foundation, G.R. Johnson and W.H. Cook proposed a fracture model [3] five years later with $I_1$, $J_2$, strain rate, and temperature dependence to be used with their plasticity model [19]. Although these models can be used uncoupled, the fracture model was developed to give the best predictions when coupled with the associated plasticity model published two years earlier [3]. The Johnson-Cook plasticity model incorporates a dynamically evolving von Mises yield criterion, dependent on equivalent plastic strain, strain rate, and temperature [19]. This model employs a so-called *strain-to-failure* principle mandating that fracture occurs only by reaching a critical level of damage, which increases from an initial value of zero to a fully damaged value of unity during plastic loading. The damage does not evolve during elastic loading or unloading. Their assumption of a von Mises yield surface implicitly dictates that plastic flow cannot occur in spherical stress states. Therefore, since the JC model allows fracture only when the material is plastically flowing, fracture will not be predicted for spherical stress states [3]. Other models, such as those proposed by Xue [8], Bao [9], and Mae [21], are also limited by the choice of a yield surface in the prediction of fracture but explicitly restrict fracture in highly hydrostatically compressive states. In contrast, the yield surface

in Kayenta [1] is much like the yield surface advocated by Mortara [22] in that it can have pressure dependence, Lode angle dependence, and a cap to allow for yielding in hydrostatic compression.

Careful consideration should be taken when using stress-based failure criteria (e.g., the JC fracture model) as their fracture predictions are extremely sensitive to the plastic hardening evolution law [7]. Unlike most of the recent stress-dependent fracture models [8, 4, 23], the JC fracture model [3] was specifically designed for use with the Johnson-Cook plasticity model [19]. However, Johnson-Cook plasticity was developed to be a computationally tractable, general high-strain rate material model; Johnson states that specialized models for specific materials will likely be more predictive [19]. Spurious results for both the stress state and the point of material failure in general loading could result from an improper or incompatible choice of constitutive models, especially when those models are designed for proportional loading (the ratio of stresses remains constant) but are neither parameterized nor applied in proportional loading situations. Even when running JC fracture and plasticity together for an applicable material, the JC model is still prone to predict fracture after it is experimentally observed to occur [3].

Johnson [19] stated that the strain hardening parameter had the greatest effect on the outcome of axisymmetric loading predictions. Castellanos [24] corroborated this assertion via a sensitivity study of the Johnson-Cook plasticity model for a broad range of load paths. Specifically, for penetration problems, the crater depth and radius, as well as the yield surface evolution, were highly dependent on the coefficient of the equivalent plastic strain. This study, along with Bishop's observation [7] of stress-based, cumulative-damage fracture models being highly sensitive to yield surface evolution, shows the precarious nature of this class of fracture models.

## 3.2 Recently Proposed Fracture Models

The importance of $J_3$ dependence in fracture models is demonstrated for metals [6, 25, 26], soil [27], and rock [28, 22]. Coppola [25] has independently determined that the deviatoric cross section of the limit surface for steel resembles the Gudehus octahedral yield profile ($J_3$ dependence), which is available in Kayenta [1].

While the dependence of $J_2$ on damage evolution is widely accepted, determining the actual stress state in an experiment is nontrivial. One example of this is the standard uniaxial tension test. This test induces nonuniform and nonuniaxial stresses when necking commences [29, 26]. This effect poses great difficulty in estimating the stress state of the plastically deforming, necking material. The general consensus is to simulate the

experiment with the boundary conditions prescribed by the experimental data and iterate until the material response in the simulation is the same as that in the experiment [26]. This approach introduces errors through the choice of model used to simulate the material and the assumptions made in the theory for that model (such as spatially and/or temporally uniform material properties like elastic moduli, and the yield stress).

Work has been done by Wierzbicki and collaborators at the Massachusetts Institute of Technology to refine the Bao-Wierzbicki and Xue-Wierzbicki (XW) fracture models [4, 13, 23, 8, 21]. However, at each iteration of development of their models, the mathematical form of their fracture locus is modified without convincing physical arguments. Nearly all of these models have been compared to the quasistatic, isothermal version of the JC fracture model. This comparison could be justified by a statement made by Johnson that, of all the material state dependencies of the JC fracture model, the stress triaxiality (which quantifies the relative magnitudes of pressure and shear stress) has the most dominant effect on ductility [3].

The majority of the fracture models being produced by Wierzbicki's group have not been validated beyond proving that their models can accurately predict fracture for the special case of the experiments used to calibrate the model. The XW fracture model [8] is the exception with some validation in the peer-reviewed literature [26], as well as some that Teng [6] performed by applying the XW model to Taylor impact experiments. However, the validation by Teng is cursory in nature with only a single reference to experimental work and is mostly a comparison of the XW fracture model against the JC fracture model. Teng's model comparison (without compelling validation) is referenced by Mae [21] as justification for the Bao-Wierzbicki fracture locus cutoff. The authority of Teng's comparative claims are questionable as all of the simulations he presented [6] show a strong mesh dependence and offered no discussion of sensitivity to mesh resolution or orientation (see Ref. [30] for experimental data of Taylor anvil tests with nonsymmetric petalling effects). Xue's own validation lacks experimental evidence beyond pointing out physical trends and comparing with simulations done by other researchers. Also, the aggregate simulated setup for each simulation has at least one plane of symmetry while the physical response is nonsymmetric about this plane. In two of the figures where the initial mesh is shown, the mesh asymmetry is obvious; the asymmetry of the material response is likely due to this mesh asymmetry (as no mention was made of seeding crack initiation). Also, there is no evidence of mesh-refinement studies or comments on convergence of the solution.

Inattention to mesh sensitivity (*e.g.,* Teng [6] and Xue[8]) is a well-known, but rarely

openly discussed, shortcoming that is rife in the literature concerning damage models. One notable exception is an article by Timmel [5], which demonstrates compellingly that fracture patterns in axisymmetric impact can be manipulated to essentially follow mesh texture. He is incredibly forthright in demonstrating the dependence of the predicted fracture pattern on mesh topology and does so in a way that is unparalleled in the literature. Brannon and Strack [31] have suggested that the mesh sensitivity of fracture can be minimized by incorporating aleatory uncertainty in material strength and have demonstrated this on a dynamic indentation problem.

Bao states [9] that his upsetting tests "proved conclusively that there is a cut-off value $\sigma_m/\underline{\sigma} = \eta = -1/3$ below which fracture will never occur..." Accordingly, the Bao-Wierzbicki fracture model [9], which is based on the CESF model, does not allow fracture for stress states below a stress triaxiality of $\eta = -1/3$ (which corresponds to uniaxial compression). The claim that the supporting data were "conclusive" is questionable, however, since it was based on only five data points.

Mirone [26] performed validation tests for the Tresca failure criterion, the Bao-Wierzbicki [9] fracture model, and the XW [4] fracture model for tensile-dominated tests. He found little difference in the predictiveness of Wierzbicki's models for simulations of round smooth and notched bars and notched plates in tension. Mirone's research shows that, for these types of tensile experiments, the $J_2$ dependence (or lack thereof) in these particular fracture models has little bearing on fracture behavior in the simulation. This demonstration shows that more complicated fracture models are not guaranteed to give better results, especially for the well-studied, ubiquitous tension test. Mirone also observes that the Tresca failure criterion does not perform well in predicting failure, which directly contradicts Wierzbicki's observation [4].

Most of the fracture models produced by Wierzbicki's group have a fracture cutoff based on the work by Bao. However, there is one exception where Xue [8] does not explicitly state the basis of his model (the XW fracture model). The first published article including the Xue-Wierzbicki model was Ref. [4] in 2005, but the article detailing the model [8] was not published until 2006 and included many modifications. One of these changes was a movement of the original cutoff value of $\eta = -1/3$ (which, recall, corresponded to uniaxial compression and was at least supported by *some* experimental data) to a new compressive fracture cutoff at $\eta = -2/3$ (which corresponds to a state of biaxial compression, and was apparently introduced without any supporting data). Even though Xue used Bao's conclusion in a past publication detailing the same model [4], Xue does not address why

the fracture cutoff is placed at this stress state or why he no longer included Bao's assumed triaxiality cutoff value [8].

The XW fracture model was designed for tensile-dominated stress states [25] and uses the findings of Bao [9] to justify neglecting the compressive domain in the validation of their model. Barsoum [32] performs independent evaluation of the $J_2$ and Lode angle dependence of the fracture locus for Weldox 420 and Weldox 960. Overall, the trends found for Weldox are very similar to the trends observed and reported by Wierzbicki [4] for Aluminum. However, the peak in strain-to-failure around a triaxiality value of $\eta = 0.8$ does not agree with the peak value seen by Wierzbicki [4] and Xue [8]. By explicit mesoscale simulation [33] of a periodic unit cell consisting of a single void in an idealized matrix, the functional form of the cumulative strain at failure as a function of Lode angle has been found to be parabolic in $\xi$, as postulated by Xue [8]. To date, however, no work has been done to address the effect of void interaction and irregular spatial distributions on the functional form of the fracture locus.

## 3.3 Summary

While much research has been focused on increasing the predictiveness of fracture models, there are serious hurdles in the application of these models including sensitivity to the hardening function [7] and mesh sensitivity [5]. Recently, there have been many fracture models proposed which explore different functional forms for stress-dependent rate of damage. In the literature [13, 9, 8], these models are typically implemented using a user-defined model in LS-DYNA or similar FEM code, which is then applied to only small verification or model calibration problems. Such models have not been ported to a massively parallel research code, a necessary step to assess the merits of the theories being proposed to solve large-scale problems in combination with other advanced constitutive theories and/or solvers.

# CHAPTER 4

# FRAMEWORK IMPLEMENTATION

One of the objectives stated in the introduction is to implement a fracture framework into Kayenta that can mimic strain-to-failure damage models. This chapter discusses how this was accomplished and which equations were used. Source code is given in Appendix A. The appendix also contains comments about what is required from the code developers and how different variables are used, as well as how extremes in strain rate and stress are handled.

## 4.1 Accumulated-Damage Framework Development

The new fracture framework is required to interface between the strain-to-failure fracture models and Kayenta's preexisting softening routine. The original framework uses a time-to-failure method suited for approximating the strain-to-failure behavior of the Johnson-Holmquist I and II models [34] when both approaches are applied at the same strain rate. By definition, and consistent with observations, a time-to-failure model predicts a lower strain-to-failure when it is applied at lower strain rates. The purpose of this research is to implement classical and contemporary strain-to-failure models in a time-to-failure softening framework so that advantages of both approaches can be realized.

The framework accomplishes this goal by dynamically setting the time-to-failure `TFAIL` at every time step for each element based on the strain rate of the element. For the constant equivalent-strain-to-failure (CESF) fracture model, this approach requires values for the equivalent plastic strain at failure $\underline{\varepsilon}^f$, the current equivalent strain $\underline{\varepsilon}^p$, the amount of time spent on the limit surface `TGROW`, and the equivalent strain rate $\dot{\underline{\varepsilon}}^p$ to calculate the output `TFAIL`. Specifically,

$$\texttt{TFAIL} = \texttt{TGROW} + \frac{\underline{\varepsilon}^f - \underline{\varepsilon}^p}{\dot{\underline{\varepsilon}}^p} \tag{4.1}$$

If the strain rate were constant, `TFAIL` would not need to be updated at every time step since, by design, this method results in an equivalent plastic strain at failure exactly equal

to $\underline{\varepsilon}^f$ if the strain rate $\underline{\dot{\varepsilon}}^p$ is constant and the stress trajectory forms a constant angle with the yield surface. Essentially, this method evaluates one iteration of the Newton-Raphson method to find an estimate for `TFAIL` at each time step for each element.

Converting strain-to-failure to time-to-failure can be alternatively formulated in terms of damage, provided that damage may be written as a function of equivalent plastic strain. Some commonly used damage models, such as Johnson-Cook fracture, define a damage variable $\mathcal{D}$ such that $\mathcal{D}$ is initially assigned a value of zero and then is allowed to increase monotonically up to a value of unity; in many of these models, no loss of strength or stiffness occurs until $\mathcal{D} = 1$. This approach can be contrasted with cohesive-type models that might also use a parameter called damage, but which predict material degradation even when $\mathcal{D} < 1$.

## 4.2 Implemented Fracture Models

The models of interest may all be viewed as belonging to the linear accumulation of damage class of models. Models of this class update damage according to

$$\mathcal{D} = \sum \frac{\Delta \underline{\varepsilon}^p}{\underline{\varepsilon}^f} \tag{4.2}$$

where the strain-to-failure $\underline{\varepsilon}^f$ may be a time-varying value and depend on stress, stress rate, strain, strain rate, temperature, *etc.*

This research aims to modify the Kayenta framework to allow the user to mimic a variety of strain-to-failure models. This is illustrated by the addition of one contemporary and two classical strain-to-failure fracture models. These three models are distinguished by their theories for setting a value to $\underline{\varepsilon}^f$:

- Constant Equivalent-Strain-at-Failure: strain-to-failure is, as the name implies, a constant given by a user-supplied parameter $D_1$.

$$\underline{\varepsilon}^f = D_1 \tag{4.3}$$

- Johnson-Cook Fracture [3]: strain-to-failure is a function of a dimensionless pressure-stress ratio $\sigma^*$ (which we have been referring to as stress triaxiality $\eta$), a dimensionless strain rate $\dot{\varepsilon}^*$ (i.e., normalized by a reference strain rate $\dot{\varepsilon}_0$), and a dimensionless homologous temperature $T^*$.

$$\underline{\varepsilon}^f = \left[D_1 + D_2 e^{D_3 \sigma^*}\right] \left[1 + D_4 \ln \dot{\varepsilon}^*\right] \left[1 + D_5 T^*\right] \tag{4.4}$$

$$\sigma^* = \frac{\sigma_m}{\sigma_e} \qquad \dot{\varepsilon}^* = \frac{\dot{\varepsilon}}{\dot{\varepsilon}_0} \qquad T^* = \frac{T - T_{\text{room}}}{T_{\text{melt}} - T_{\text{room}}} \tag{4.5}$$

  In these formulas, the eight user-supplied parameters are $D_1 ... D_5$, $\dot{\varepsilon}_0$, $T_{\text{melt}}$, and $T_{\text{room}}$.

- Xue-Wierzbicki Fracture [4]: strain to failure depends on stress triaxiality $\eta$, and the Lode parameter $\xi$.

$$\underline{\varepsilon}^f = D_1 e^{-D_2\eta} - \left(D_1 e^{-D_2\eta} - D_3 e^{-D_4\eta}\right)(1-\xi^m)^n \tag{4.6}$$

$$\xi = \frac{27}{2}\frac{J_3}{\underline{\sigma}^3} \qquad \eta = \frac{\sigma_m}{\underline{\sigma}} \qquad m = 2 \text{ Round}\left(\frac{1}{2n}\right) \tag{4.7}$$

  Here, the five user-supplied material parameters are $D_1 ... D_4$ and the hardening exponent $n$ (which is assigned the same value as the hardening exponent used in power law plasticity theory).

The full documentation (and commentary) for each of these models includes special restrictions that must be satisfied to apply these formulas and should be extensively researched to determine if any of these models are applicable to a given situation.

Modification of Kayenta to include a strain-to-failure ability without disrupting its existing time-to-failure framework is straightforward. In particular,

$$\texttt{TFAIL} = \frac{(1-\mathcal{D})\underline{\varepsilon}^f}{\dot{\underline{\varepsilon}}^p} + \texttt{TGROW} \tag{4.8}$$

Here, the value of $(1-\mathcal{D})\underline{\varepsilon}^f$ is simply the remaining equivalent plastic strain before failure according to the current material state and loading rate.

The value of $\underline{\varepsilon}^f$ can change with respect to the stress state. However, Kayenta supports viscoplasticity and tracks the quasistatic stress and the dynamic stress concurrently. The quasistatic stress always resides within the limit surface while the dynamic stress is not confined by the limit surface. Only when viscoplasticity is used do these two stress values differ. Because of these two potentially different stress values, one of them must be chosen for use in these newly implemented models. At high rates, the dynamic stress is the actual stress being carried by the element, making it the preferred choice for the stress-dependent strain-to-failure theory. However, Kayenta does not currently support viscoplasticity with softening, but that functionality will likely be allowed in the future.

## 4.3 Special Cases

For loading conditions that change significantly from time step to time step, there are two safety checks that ensure the softening proceeds as would be expected for a purely strain-controlled mechanism. The first check is a requirement of `TFAIL` to remain constant after the first instance of `TGROW` exceeding `TFAIL`. Keeping `TFAIL` constant is required to maintain a gentle decrease in `COHER` (which may be an issue when `TFAIL` is a function of

the stress state). The second check is a requirement that COHER not increase between time steps. This ensures that spurious oscillations of material softening and healing not occur.

The effects of these checks can be be described in relation to Figs. 4.1 and 4.2, which contains the time history of a single element simulation. The effect of the first check is visible in the more gradual decrease in COHER after fracture has occured. The effect of the second check cannot be seen in the single element test contained in Fig. 4.1. A commmon artefact of the second check is a plateau of COHER after it has begun to drop but before it reaches zero.

## 4.4 Code Requirements

This new framework requires several new state variables to be tracked to correctly predict material failure. The original softening routine in Kayenta requires only two material constants: TFAIL and FSPEED. The associated memory requirement is minimal, just two double-precision floating points variables. However, for this wrapper to be used,

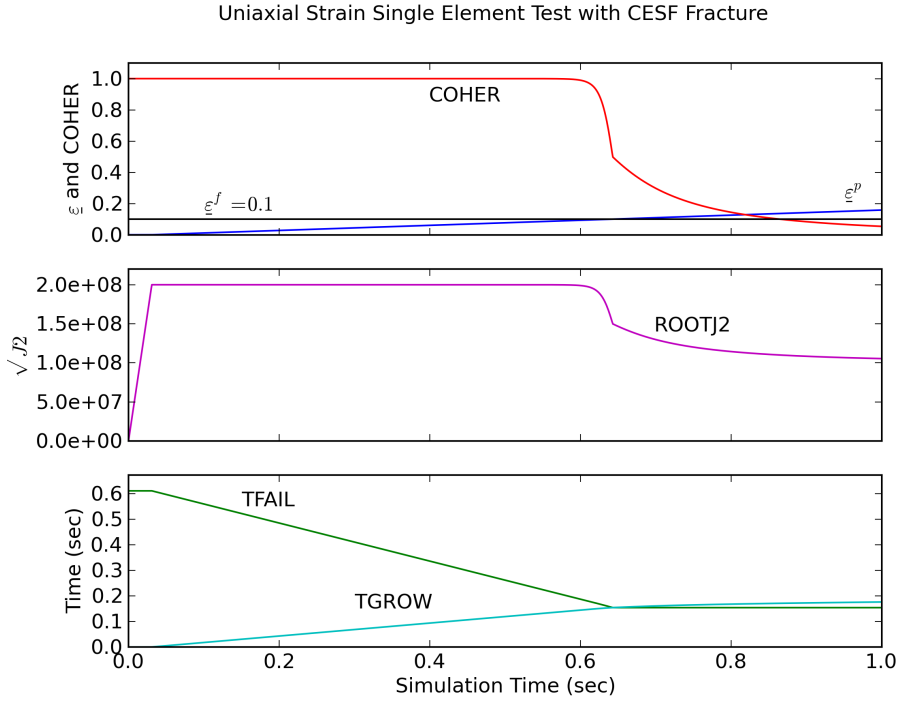


**Figure 4.1**: Here is an example of the evolution of the internal state variables for a uniaxial extension single element simulation using the constant equivalent-strain-to-failure fracture model. Strain is linear with time. The black horizontal line denotes the strain at which fracture is expected to occur. As can be seen, when COHER = 0.5, TGROW is equal to TFAIL and the equivalent strain is equal to the analytic value of strain at failure. Notice the sharp change in slope of COHER, TGROW, and ROOTJ2 when fracture is predicted. This is caused by the changing direction of the stress trajectory with respect to the collapsing limit surface.

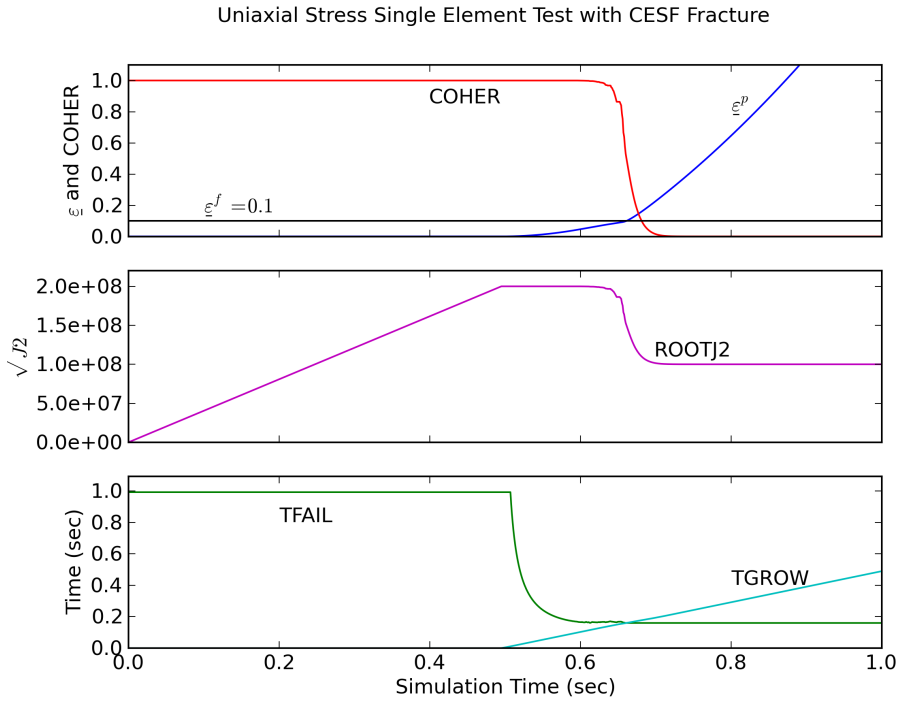


**Figure 4.2**: Here is an example of the evolution of the internal state variables for a uniaxial tension single element simulation using the constant equivalent-strain-to-failure fracture model. Stress is linear with time. The black horizontal line denotes the strain at which fracture is expected to occur. As can be seen, when `COHER` $= 0.5$, `TGROW` is equal to `TFAIL` and the equivalent strain is equal to the analytic value of strain at failure.

two new state variables are required to correctly track the material state. The new state variables track the fracture damage (`FDAMAGE`) and time-to-failure (`TFAIL`) for each element. Together, these state variables require $2n$ doubles to be stored for the simulation as a whole, where $n$ is the number of elements. For comparison, the basic build of Kayenta without the orthotropic or anisotropic options has nearly fifty state variables (requiring $50n$ doubles) without these additions.

For simulations where the Johnson-Holmquist I or II models or no softening behavior is desired, the new state variables are initialized to zero and to the user-specified `TFAIL`. To minimize the amount of movement between memory and processor cache, they are not referenced again. This implementation minimizes the impact on runtime when these damage models are not in use.

## 4.5 Conclusion

The new fracture framework has been implemented to minimize impact on the original layout and performance of Kayenta. This has been done by dynamically setting `TFAIL` in

such a way as to predict failure when $\underline{\varepsilon}^p = \underline{\varepsilon}^f$.

This new framework can be simply extended for newer fracture models that are of the class of models with linear accumulation of damage. Because Kayenta is currently in many host codes, researchers will be able to apply these models to large-scale, complex problems without the time requirement associated with the implementation of a new model into their host code.

# CHAPTER 5

# VERIFICATION

Any constitutive model, no matter how long it has been in use, should undergo regular verification and validation testing. Verification, in this sense, refers to the act of ensuring that the model has been correctly implemented and connected to the host code while validation ensures that the model's predictions match experimental observations. The importance of verification testing for all usage conditions cannot be overstated. Verification testing proves that a model's predictions can be trusted for the specific usage scenarios where the constitutive assumptions are met. However, when a model is not implemented correctly, its results cannot be trusted; the only way to build confidence in a model is to do verification testing. Ideally, verification testing is done by using the constitutive equations to derive an analytical solution and compare that to the computed approximation to make certain that the model is behaving appropriately. Even when analytical solutions are not tractable, verification testing is applied to confirm expected trends in the results and appropriate numerical behavior such as convergence and stability.

For this research, an integral part of which is to enable fast prototyping of recently developed fracture models with linear accumulation of damage, verification is of the utmost importance as this research lays a foundation for future models to be implemented. Specifically, the new strain-to-failure damage framework (along with the three initial models to be included: the constant equivalent-strain-to-failure (CESF), Johnson-Cook [3] (JC), and Xue-Wierzbicki [4] (XW) fracture models) is being implemented into Kayenta [1], a computational framework for generalized plasticity models. Kayenta was a natural choice for this research as it is already part of numerous codes in use by private companies and government laboratories domestically as well as abroad. Because Kayenta is already in daily use by many researchers and is installed on many clusters, some of them frequently utilizing thousands of processors per simulation, these models can be implemented and evaluated in large-scale applications with very little time spent on the model/host code interface. However, before running simulations with millions of elements, it is necessary to

do extensive single-element testing.

Kayenta's primary benchmarking and single-element testing framework is called Payette [35]. Payette is a flexible, easily extensible framework written in Python that supports a user-defined mixture of stress and strain control, as well as a user-defined electric field (for ferroelectric and piezoelectric models). Because of the great flexibility and ease of use of Payette, it is adopted in this research to verify the implementation of these three fracture models into Kayenta. In the case of the JC and XW fracture models, it is very important to maintain proportional loading along a constant stress triaxiality and Lode angle (which corresponds to the set of stress states falling on a straight line passing through the origin in Haigh-Westergaard space). Because the verification problems that we are looking at involve softening (loss of shear strength), it is very difficult to maintain proportional loading throughout the simulation while maintaining a nonzero strain rate because of the collapsing limit surface.

Given that constitutive models are invariably written such that strain or strain increment is the input, with updated stress and internal variables being the outputs, Payette can iteratively solve an inverse problem to determine the strain increments required to achieve a prescribed stress or stress increment. In the verification plots to follow, it will be seen that Payette performs well in prescribed-stress proportional loading cases of triaxial extension, triaxial compression, and pure shear. However, maintaining proportional loading for stress states that are not in the preceding list is much more difficult for specific values of stress triaxiality. Artifacts from this shortcoming of Payette (not Kayenta or the implementation of the fracture framework) can be identified by excessive noise in the `EQPS` value at a given `COHER` value. Figure 5.4 (which will be shown later) depicts this instability well as all the failure strain realizations from the single element tests for the CESF model should be at an intersection of the grid lines representing the analytical solution.

The verification tests in this chapter are analyzed in much the same manner as the laboratory tests used to calibrate the Xue-Wierzbicki model [4]. Also, these analyses use the user inputs that Wierzbicki proposed for Aluminum 2024-T351 and are included in Table 5.1. In particular, most of the verification tests in this chapter are performed on states of plane stress since Weirzbicki states that all of his specimens failed in states of plane stress. The primary measurement from a given simulation or experiment is the equivalent plastic strain at failure. Wierzbicki [4] makes the assumption that all strains (volumetric and deviatoric, elastic and plastic) are plastic, but classic fracture models (e.g., the JC [3] and Wilkins [20] fracture models) use only the deviatoric part of the plastic strain to compute

**Table 5.1**: A list of values used to parameterize the models for the verification plots. The fracture models all used parameters published in Ref. [4]. All values in MKS.

| Material Parameters for Al 2024-T351 | | | | | |
|---|---|---|---|---|---|
| von Mises | $K$ | | $G$ | | $Y$ |
| | $71.5 \times 10^9$ | | $28 \times 10^9$ | | $283 \times 10^6$ |
| CESF | $\underline{\varepsilon}^f$ | | | | |
| | 0.21 | | | | |
| JC Fracture | $D_1$ | $D_2$ | $D_3$ | $D_4$ | $D_5$ |
| | 0.13 | 0.13 | -1.5 | 0.0 | 0.0 |
| XW Fracture | $D_1$ | $D_2$ | $D_3$ | $D_4$ | $n$ |
| | 0.87 | 1.77 | 0.21 | 0.01 | 0.153 |

the equivalent plastic strain. Because of this precedent, the Kayenta implementation of the three fracture models will be based on the equivalent deviatoric plastic strain.

Equivalent strain at failure is often plotted against the two most likely independent variables, namely the stress triaxiality and the Lode parameter. These two values loosely represent $J_2$ and $J_3$ dependence, respectively. While the dependence of fracture on $J_2$ is well known, current publications are increasingly reporting that $J_3$ dependence is nonnegligible for fracture prediction.

Though some research efforts using servo-controlled axisymmetric loading have shown promise in achieving controlled movement of the stress state through stress space [36], triaxiality and the Lode parameter are difficult to keep constant during laboratory tests. Because of this, the averages of both the triaxiality and Lode parameter are computed (in both the experiment and simulated analysis) through an equivalent-strain-weighted average:

$$\eta_{\text{avg}} = \frac{1}{\underline{\varepsilon}^f} \int_0^{\underline{\varepsilon}^f} \eta \, d\underline{\varepsilon}^p \tag{5.1}$$

$$\xi_{\text{avg}} = \frac{1}{\underline{\varepsilon}^f} \int_0^{\underline{\varepsilon}^f} \xi \, d\underline{\varepsilon}^p \tag{5.2}$$

The XW and the quasi-static, isothermal JC fracture models both assume proportional loading to failure for the analytical solution to be valid. As Wierzbicki and others have used the strain-weighted average technique to parameterize the models, we will use it to include the effects of slight nonproportional deviations in loading for the single-element tests.

In many of the verification figures to follow, there is a comparison of the effect of `FSPEED` on the accuracy of the fracture prediction. As discussed earlier, `FSPEED` controls how

quickly the material loses strength; low values of FSPEED dictate that softening proceeds slowly while large values implies near-instantaneous softening. The gradual nature of the loss of strength calls into question when, precisely, a material transforms from intact to fractured. The upcoming figures and discussion compare the value of plastic strain when COHER $= 0.5$ with the failure strain $\underline{\varepsilon}^f$ in the three fracture models. For each single-element test reported in the upcoming figures, there are three points that convey the range over which the material is softening. As the loss of strength occurs over relatively few time steps, we use a linear interpolation of the independent variable COHER to determine the equivalent plastic strain at exact values of coherence. Time step size has been reduced to help in minimizing errors from the linear interpolation, but some small amount of error still exists.

To generate plane stress states, the ratio of the nonzero stresses was determined by realizing a distribution of equally spaced angles ranging from $[\pi/4, 5\pi/4]$ and using each angle realization $\phi$ in

$$\frac{\sigma_1}{\sigma_2} = \frac{\cos\phi}{\sin\phi} \tag{5.3}$$

This gives a ratio of unity for both $\pi/4$ and $5\pi/4$, which correspond to biaxial tension and biaxial compression, respectively (see Table 2.1). Because the material is isotropic, it is not necessary to generate angle realizations for the full circle. However, the framework has been tested extensively to verify that material isotropy is maintained. For states of plane stress with the ratio of the nonzero stresses as defined above, the stress triaxiality $\eta$ is given by

$$\eta = \frac{\cos(\phi) + \sin(\phi)}{3\sqrt{1 - \frac{1}{2}\sin(2\phi)}} \tag{5.4}$$

As seen in Fig. 5.1, stress triaxiality $\eta$ is nearly linear with respect to $\phi$. However, the slight nonlinearity (especially at the extremes) will produce slightly nonuniform spacing in triaxiality realizations when the angle $\phi$ is sampled uniformly. This accounts for the minor spacing irregularities in many of the upcoming figures.

The root-mean-square error (RMS error or the standard deviation of error) is presented as a quantitative method to determine the accuracy of the framework. For each triaxiality realization, a single element simulation was performed. The analytical value of $\underline{\varepsilon}^f$ (as determined by the triaxiality realization) is compared with the simulated value of $\underline{\varepsilon}^p$ (EQPS) when COHER $= 0.5$. Thus, the RMS error encompasses the errors introduced by the proportional stress implementation of Payette as well as the fracture framework error.

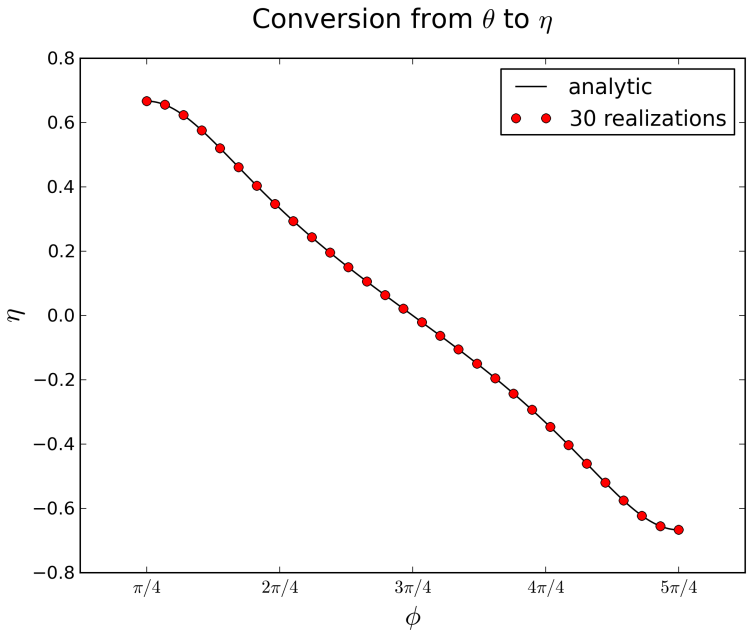


**Figure 5.1**: A comparison of triaxiality versus proportionality angle for plane stress states.

## 5.1 Constant Equivalent-Strain-at-Failure Verification

The scatter evident in Fig. 5.2, where `FSPEED` = 5, is caused by the previously mentioned difficulty of maintaining proportional loading for those particular values of the Lode parameter. When `FSPEED` = 50 the accuracy and precision of predicted equivalent plastic strain at fracture are much increased, giving excellent agreement with the analytical solution (in this case $\underline{\varepsilon}^f = 0.21$, shown by the black line) considering that, during the loss of strength in prescribed stress simulations, strain rate increases dramatically. The RMS error between the analytical solution and the `EQPS` values when `COHER` = 0.5 and `FSPEED` = 50 in Fig. 5.4 is 0.000059, or approximately 0.03%. This model is a very good indicator of the overall accuracy of the fracture framework, especially as it is a simple model without peaks or cusps in $\underline{\varepsilon}^f$ versus $\eta$ and $\xi$ space.

As previously mentioned, the triaxiality realizations were generated by varying the angle $\phi$ in the plane stress ($\sigma_2$ vs. $\sigma_1$) space. As $\phi$ is varied, not only does triaxiality change, but the Lode parameter varies as well. Therefore, Figs. 5.2 and 5.3 show variation of strain-to-failure with respect to both triaxialtity and the Lode parameter.

## 5.2 Johnson-Cook Verification

As seen in Figs. 5.5, 5.6, and 5.7, the JC fracture model verification results are similar to those of the CESF model. The same difficulties in maintaining proportional loading

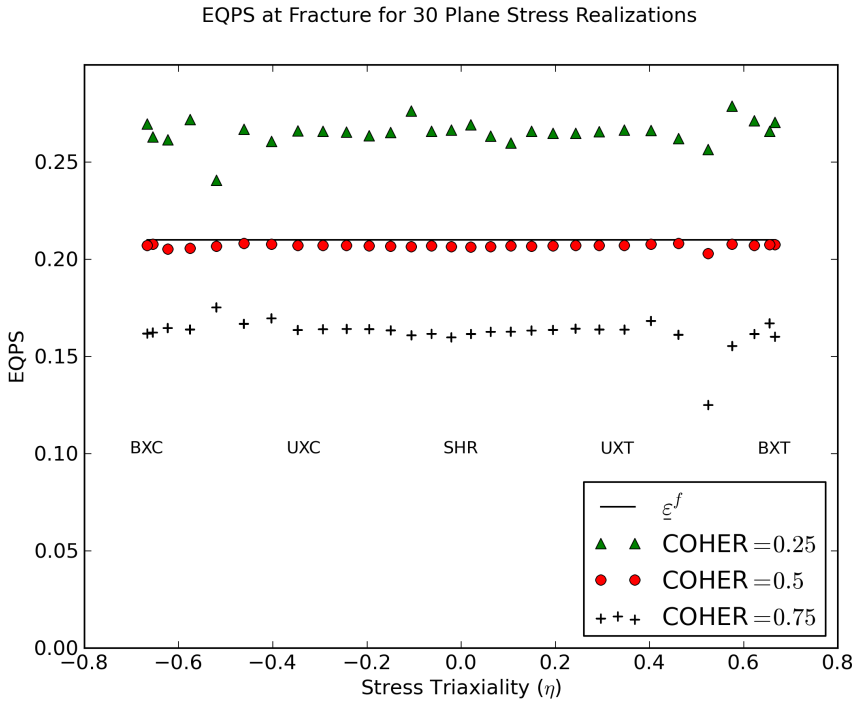


(a) FSPEED $=5$

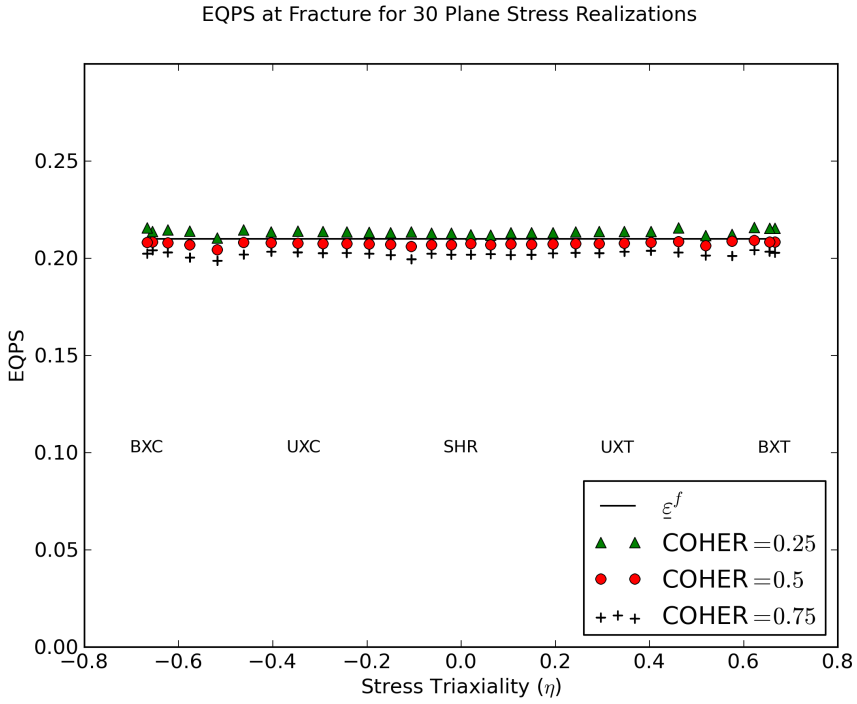


(b) FSPEED $=50$

**Figure 5.2**: Comparison of accuracies of equivalent plastic strain (EQPS) at failure for different values of FSPEED using the constant equivalent-strain-at-failure fracture model.

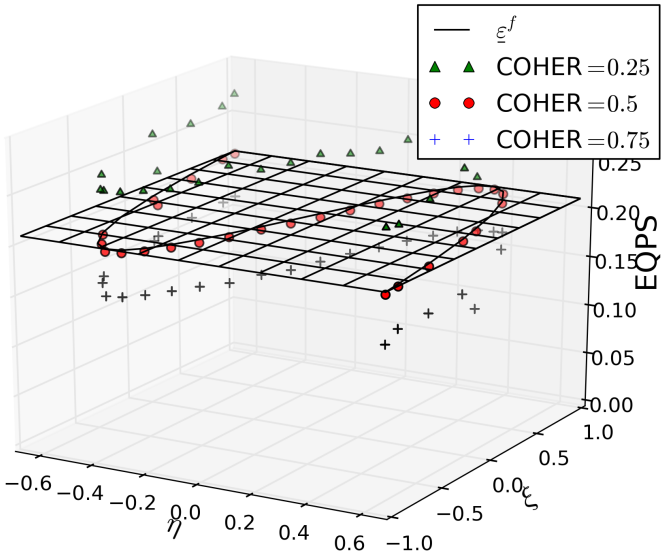


(a) FSPEED=5

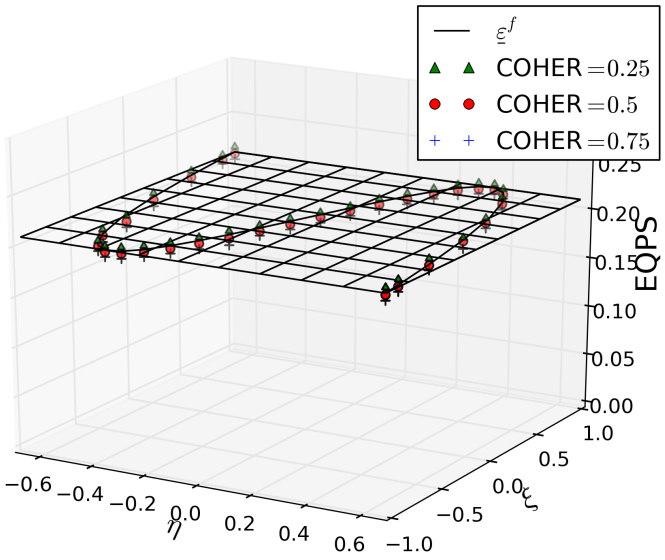


(b) FSPEED=50

**Figure 5.3**: 3D comparison of accuracies of equivalent plastic strain (`EQPS`) at failure for different values of `FSPEED` verses strain-averaged triaxiality and Lode parameter using the constant equivalent-strain-at-failure fracture model.

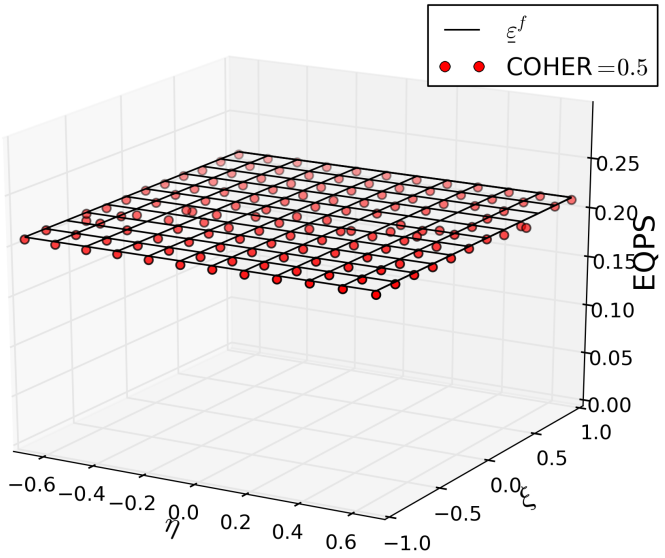


**Figure 5.4**: This plot demonstrates the limitations of Payette in maintaining proportional loading for certain values of $\eta$ and $\xi$ (with `FSPEED` $= 50$). However, for verifying the accuracy of the fracture framework, the results are very good for all points displayed (the RMS error is approximately 0.03%).

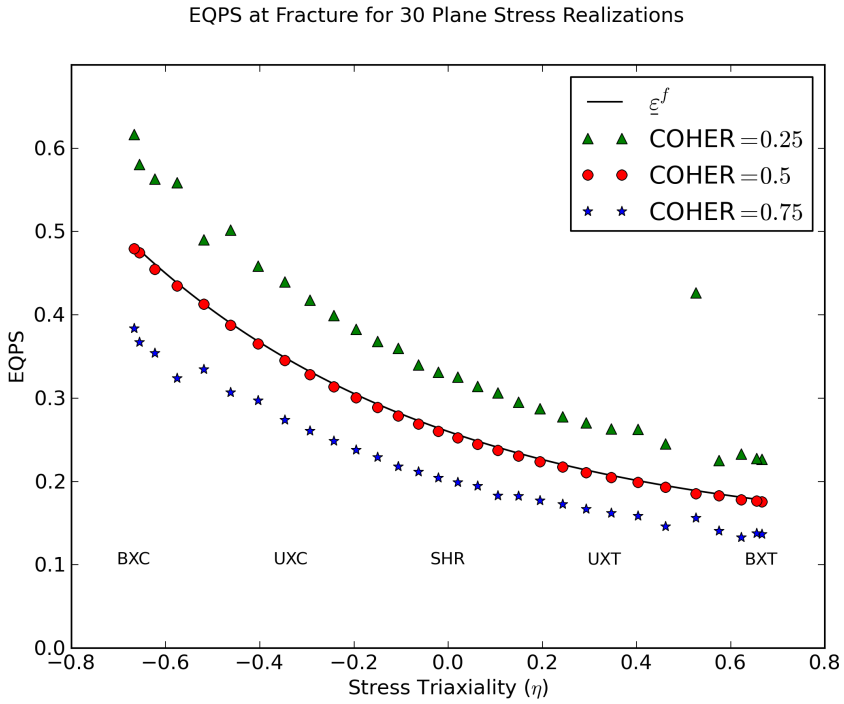


(a) FSPEED =5

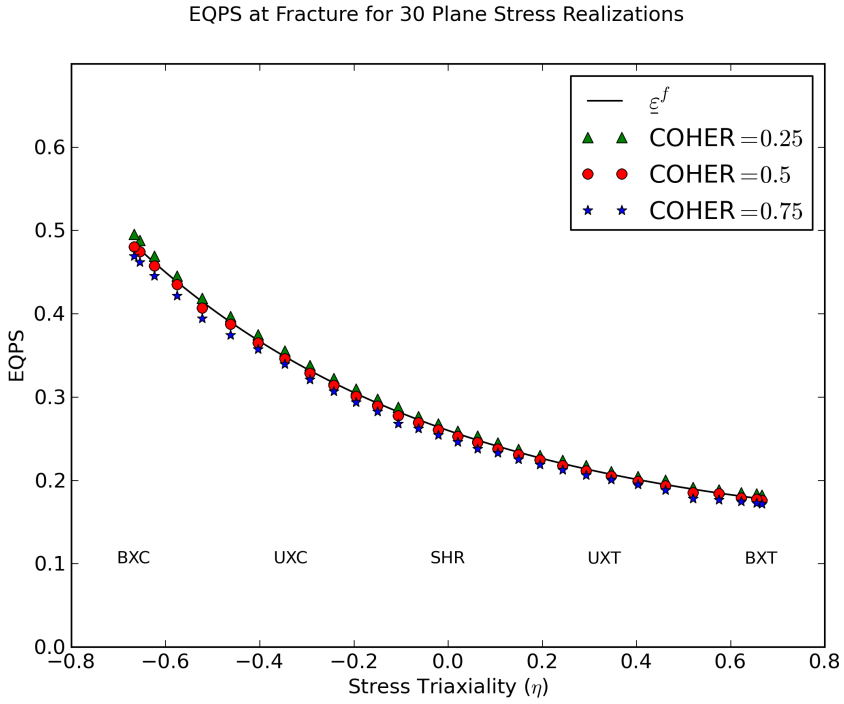


(b) FSPEED =50

**Figure 5.5**: Comparison of accuracies of equivalent plastic strain at failure for different values of FSPEED verses strain-averaged triaxiality using the Johnson-Cook fracture model.

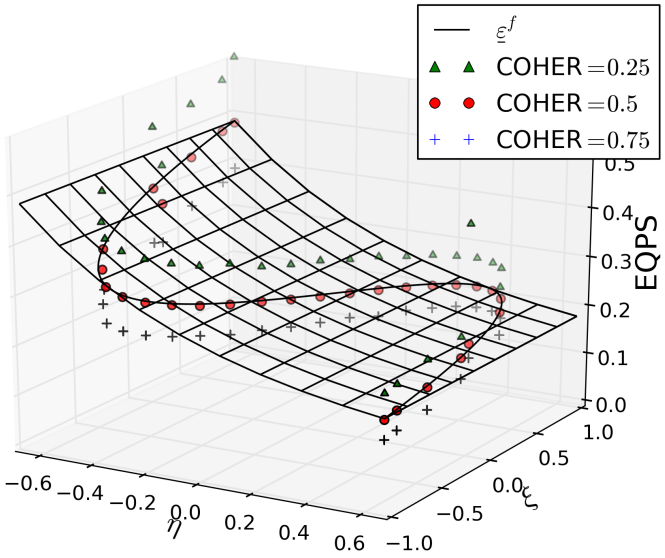


(a) FSPEED =5

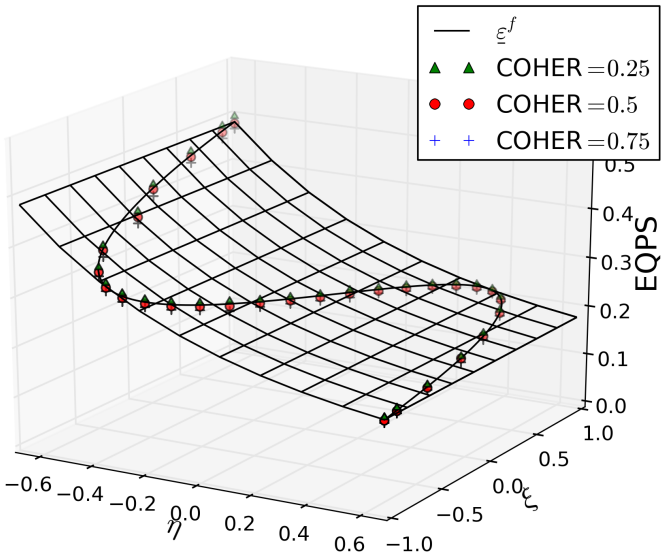


(b) FSPEED =50

**Figure 5.6**: 3D comparison of accuracies of equivalent plastic strain at failure for different values of FSPEED verses strain-averaged triaxiality and Lode parameter using the Johnson-Cook fracture model.

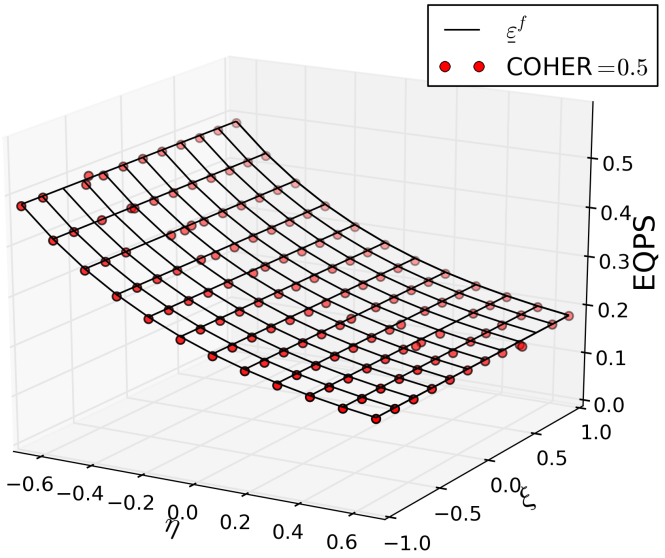


**Figure 5.7**: This plot demonstrates the limitations of Payette in maintaining proportional loading for certain values of $\eta$ and $\xi$ (with `FSPEED` $= 50$). However, for verifying the accuracy of the fracture framework, the results are very good for all points displayed (the RMS error is approximately 0.93%).

(and the corresponding scatter in predictions) are encountered, particularly for low values of `FSPEED`. The single-element tests and the analytical solution agree within a standard deviation of 0.0032. As the $\underline{\varepsilon}^f$ value varies with respect to $\eta$, this error can be approximated as 1.0% assuming an average $\underline{\varepsilon}^f$ value of 0.3. As it is necessary for the new code to be considered well-verified for these problems, the analytical solution (black line in Fig. 5.5) lies within the range of `EQPS` between `COHER` = 0.75 and `COHER` = 0.25 for the entire domain of interest. This test of the quasi-static, isothermal JC model shows that, for a more complicated model with $\eta$ dependence, the framework can still predict failure close to the analytical solution.

## 5.3 Xue-Wierzbicki Verification

The XW model posed some challenges to the verification framework. While the form of the fracture locus in $\eta$ space is functionally similar to that of the JC model, the coefficients in the exponential are much larger and predict unreasonably high fracture strains for Lode angle parameters extremely close to $+1$ or $-1$ (see Fig. 5.8; this accounts for the anomalous strain spikes in Fig. 5.9).

In the verification realizations in Figs. 5.9a, 5.9b, and 5.10 the cusps of the analytical solution are difficult to reproduce. This is due, in part, to the averaging process (see Eqs. 5.1 and 5.2) to determine the values of $\eta$ and $\xi$ to plot the computed `EQPS` against. The bulk of the cause of the discrepancies at the cusps is the linear accumulation of damage with slight deviations in $\eta$ and $\xi$. This difficulty is reflected in the RMS error (error = 0.027) between the realizations and the analytic solution. However, the `EQPS` error goes down to 0.0028 when values on the cusps ($\underline{\varepsilon}^f > 0.5$) are neglected.

Verification for the XW model at stress triaxialities below $-1/3$ is entirely academic as the model assumes a fracture cutoff at $\eta = -1/3$. As this is primarily a verification for the strain-to-failure framework, this region was included to push the limits of reasonable `EQPS` values at fracture for highly specific stress states.

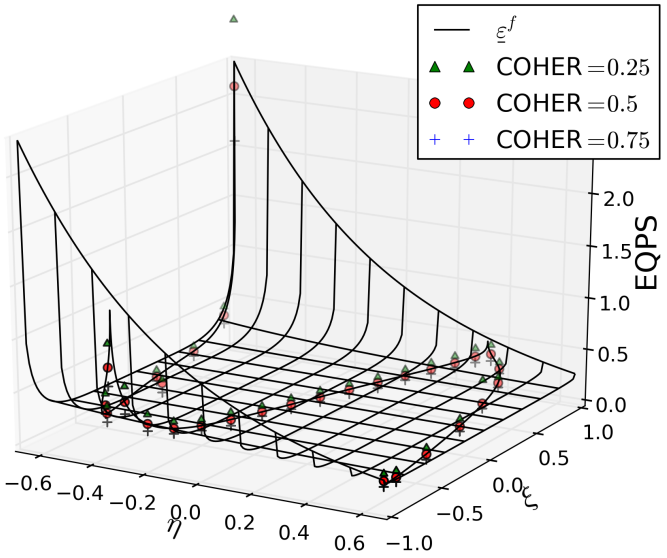


(a) FSPEED =5

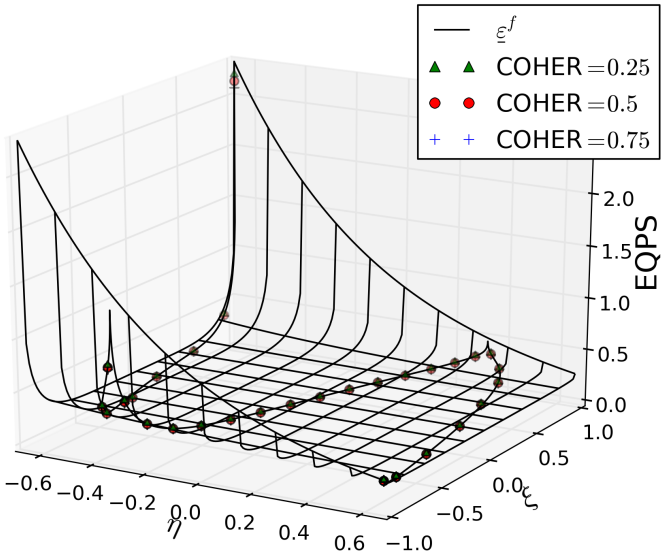


(b) FSPEED =50

**Figure 5.8**: 3D Comparison of accuracies of equivalent plastic strain at failure for different values of FSPEED verses strain-averaged triaxiality and Lode parameter using the Xue-Wierzbicki fracture model.

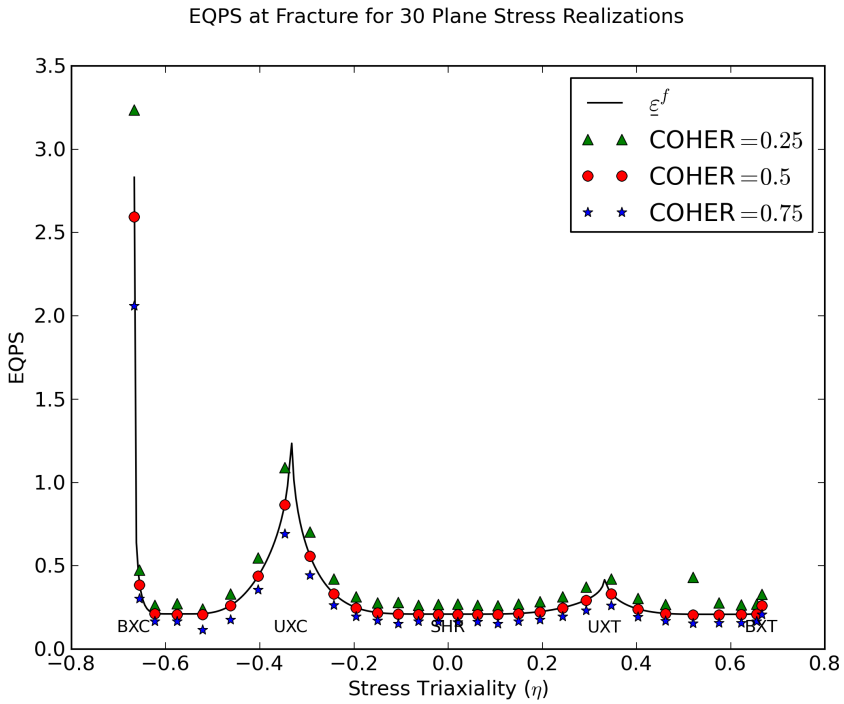


(a) FSPEED $=5$

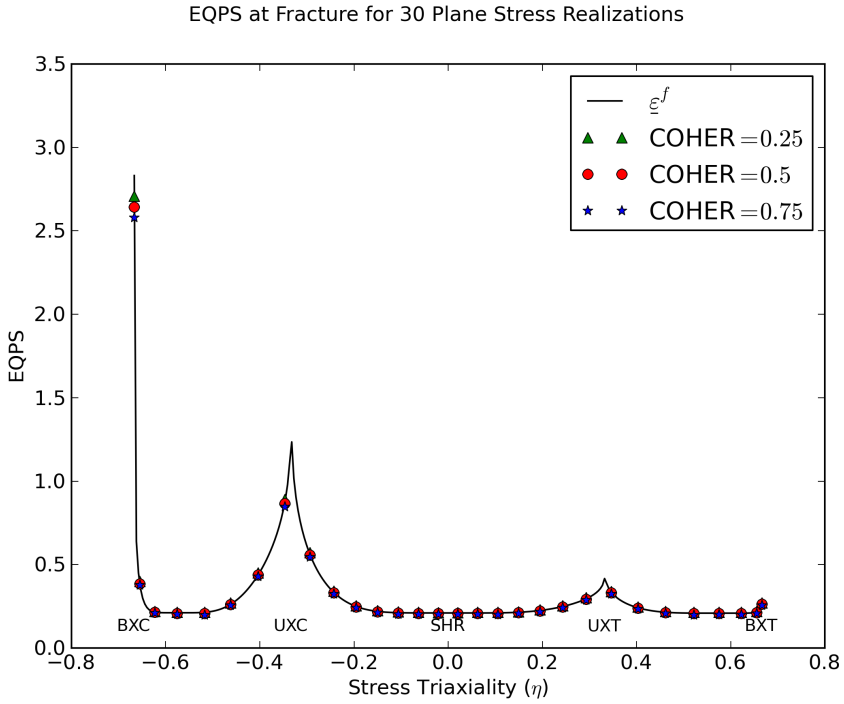


(b) FSPEED $=50$

**Figure 5.9**: Comparison of accuracies for different values of FSPEED using the quasi-static, isothermal Xue-Wierzbicki fracture model.

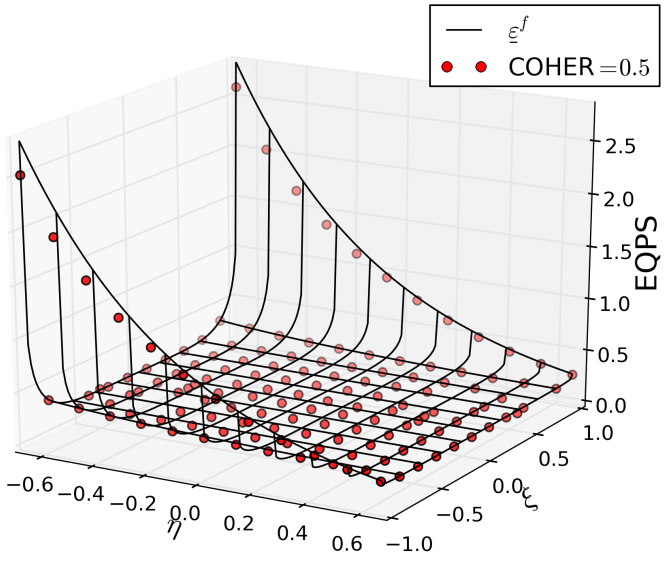


**Figure 5.10**: This plot demonstrates the limitations of Payette in maintaining proportional loading for certain values of $\eta$ and $\xi$ (with `FSPEED` $= 50$). However, for verifying the accuracy of the fracture framework, the results are very good for all points displayed (the RMS error is approximately 0.022%).

# CHAPTER 6

# VALIDATION

The scope of this research has been limited to the implementation and verification of three options for strain-to-failure in Kayenta. Separate concurrent efforts are underway to quantify the validity of these three theories as applied to the Charpy impact experiment. Rather than endorsing any of the aforementioned fracture models for any particular loading situation, this research merely aims to provide the option to explore prevailing damage theories in a common framework, which facilitates assessing the merits of these models in expanded validation testing slated for future work. The recently implemented fracture models are likely to improve the predictiveness of Kayenta for certain types of simulations. The simulation that we will showcase is that of an unnotched Charpy impact experiment on steel.

The validation simulation is to be performed on a steel specimen of dimensions 55mm $\times$ 10mm $\times$ 5.5mm being impacted on the 10mm side by a striker traveling at 50m/s. A depiction of the initial configuration is found in Fig. 6.1. The supports and striker are modeled as a very stiff, linear-elastic material. The simulation is run for 300$\mu$sec. The termination time was chosen so that the target would undergo maximum deformation without losing contact with the supports.

The models that will be compared are:

- the original Kayenta Softening model
- the constant equivalent-strain-to-failure fracture model
- the Johnson-Cook fracture model
- the Xue-Wierzbicki fracture model

Each model is applied three times to the validation simulation, each at different mesh resolution.

The experimental fracture features that we are hoping to capture are shown in Figs. 6.2 and 6.3. Specifically, the main characteristics that we wish to capture are:

- **Primary Crack Behavior** In Fig. 6.3 the cup-and-cone fracture pattern can be seen. One goal of the current research is to independently investigate the assertion by

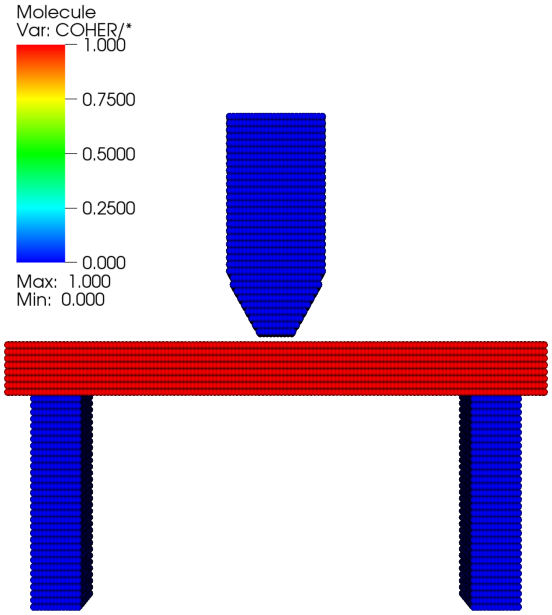


**Figure 6.1**: The unnotched Charpy simulated setup. The bar in red is the steel specimen being held in place by the supports (bottom) and impacted by the striker (top). The supports and striker are both being modeled as a perfectly elastic materials with a high elastic modulus.

Xue et al. [8] that their strain-to-failure model is able to predict a cup-cone fracture pattern that (they assert) is not predicted using standard Johnson-Cook fracture.

- **Secondary Cracks** We further hope to predict secondary cracks that do not propagate through the thickness of the specimen.

## 6.1 Parameterization

The models were parameterized, where possible, from values found in the literature or from material databases. The parameterization effort can be viewed as occurring in two distinct steps of elastic-plastic and fracture parameterization.

The elastic portion was particularly easy to parameterize. There are many resources that freely distribute the elastic moduli and the yield stress in tension. However, relatively few materials characterization databases provide multiple values at different stress states on the yield surface. The parameterization of the plastic response was explored using a linear Drucker-Prager yield surface, a power-law kinematic hardening yield surface, and


**Figure 6.2**: Six unnotched Charpy impact specimens made of steel similar to 4340 depicting the type of fracture we wish to reproduce. This image shows the side opposite that of the striker, which had a velocity of 50m/s. The smaller cracks that are parallel to the primary crack are particularly difficult to capture in the simulations. Reproduced with permission from Idaho National Laboratories.

variations on the von Mises yield surface. The goal of verification testing was to confirm that the three new fracture options were implemented correctly and that they predicted different results for the same loading paths. For this purpose, a simplistic nonhardening von Mises yield criterion was adopted to be consistent with the conventional yield model for metals.

Experimental data for edge-on-impact experiments for glass [37] demonstrate that damage velocity asymptotes to the longitudinal sound speed for the material. Presuming that similar behavior applies to metals, the original Kayenta softening model was parameterized by taking the damage speed to equal the sound speed. Then `TFAIL` was set equal to the amount of time required for a damage wave to propogate a distance given by the characteristic length (cube root of volume) of each element. Importantly, this approach imposes a

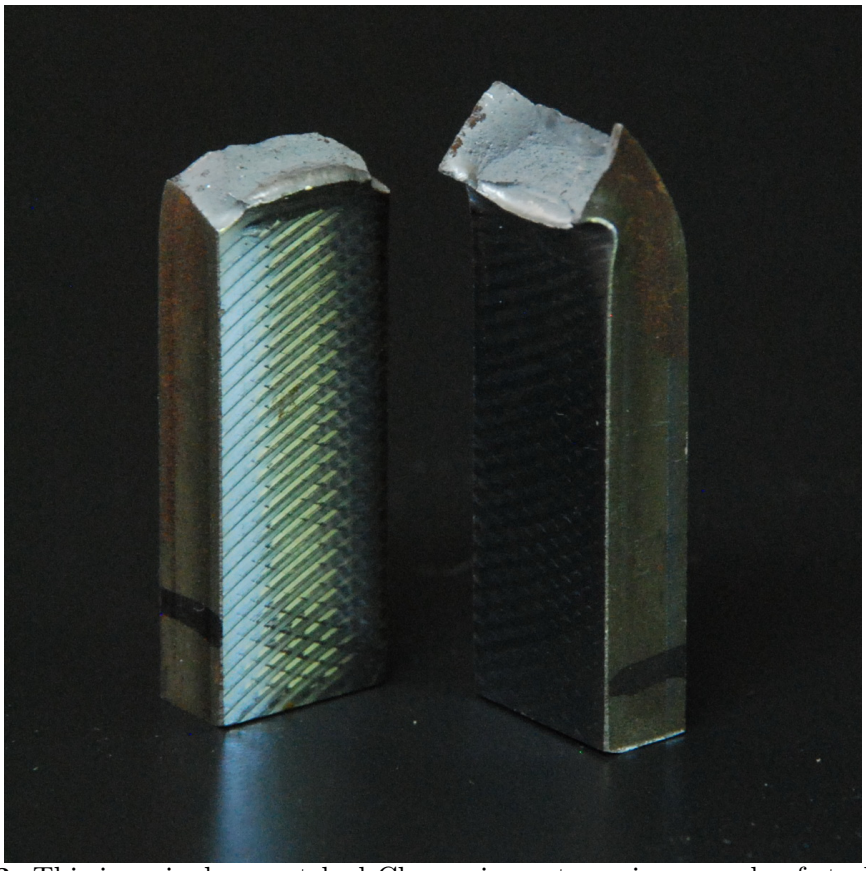

**Figure 6.3**: This is a single unnotched Charpy impact specimen made of steel similar to 4340 of the dimensions 55mm × 10mm × 5.5mm and was impacted by a striker at 50m/s. This images shows the *cup and cone* effect of fracture. Reproduced with permission from Idaho National Laboratories.

simple scale effect to the damage model. The Constant Equivalent-Strain-to-Failure model was parameterized by elongation at break data (in which there is much variance). The Johnson-Cook fracture model parameters were taken from the default values in Alegra [38] for 4340 steel (which were, in turn, taken from the CTH [39] material libraries). The Xue-Wierzbicki fracture model was parameterized by using the Johnson-Cook fracture values for two special cases. The first was that of triaxial extension (or compression) where $\xi = \pm 1$. This allows the first two XW parameters to be isolated and optimized to reproduce the JC fracture curve over the range of triaxialities $-\frac{2}{3} \leq \eta \leq \frac{2}{3}$. The fourth parameter was chosen to be zero to give an apparent constant strain-to-failure for pure shear stress states ($\xi = 0$). This assumption is based on the comparative level nature of $\xi = 0$ in Fig. 5.8 over the stated triaxiality range. Then, the JC fracture value for ($\eta = 2/3$, $\xi = 0$) was used for the third XW parameter. The strain-hardening exponent was found in a book written by Callister [40].

The following simulations were parameterized as stated above (values are given in Table 6.1) and run without "dialing in" the model parameters. After presenting the results, some discussion is given about uncertainty in reported model parameters and possible effects of choosing different values within that uncertainty.

## 6.2 Simulation Output

Each of the models used have been run with low, medium, and high mesh resolutions with 10024, 77952, and 642872 particles, respectively. The mesh resolution is doubled in each direction for each increase in mesh refinement and can be verified by noting that the ratio of the number of particles between sets is approximately 8 ($2^3$).

All of the simulations ran to completion with the exception of the high resolution run of the original Kayenta softening routine which consistently failed due to a negative Jacobian even upon time-step refinement; the simulation is shown at the time step before the code terminated with the Jacobian error. The model outputs are located in Figs. 6.4, 6.5, 6.6, and 6.7. All values in the plots are in SI units.

## 6.3 Discussion

Two unexpected results from these simulations were the failure of the original softening model to give consistent results (i.e., similar damage patterns at each mesh refinement level) and the near-complete lack of material softening for both the JC and XW fracture models. Most of the simulations show slight surface damage at the point of contact between the target and the supports, as is observed in the experiment in Fig. 6.2. However, the CESF model was the only one to give a consistent, plausible result for the primary fractures in front of the striker using failure parameters based purely on freely available data.

**Table 6.1**: A list of values used to parameterize the models for the validation simulations. All values in MKS.

| Material Parameters for 4340 Steel | | | | | |
|---|---|---|---|---|---|
| von Mises | $K$ | | $G$ | | $Y$ |
| | $173.3 \times 10^9$ | | $80 \times 10^9$ | | $676 \times 10^6$ |
| CESF | $\underline{\varepsilon}^f$ | | | | |
| | 0.25 | | | | |
| JC Fracture | $D_1$ | $D_2$ | $D_3$ | $D_4$ | $D_5$ |
| | -0.65 | 2.25 | -0.5 | 0.0004 | 0.0 |
| XW Fracture | $D_1$ | $D_2$ | $D_3$ | $D_4$ | $n$ |
| | 1.584 | 0.696 | 0.995 | 0.0 | 0.12 |

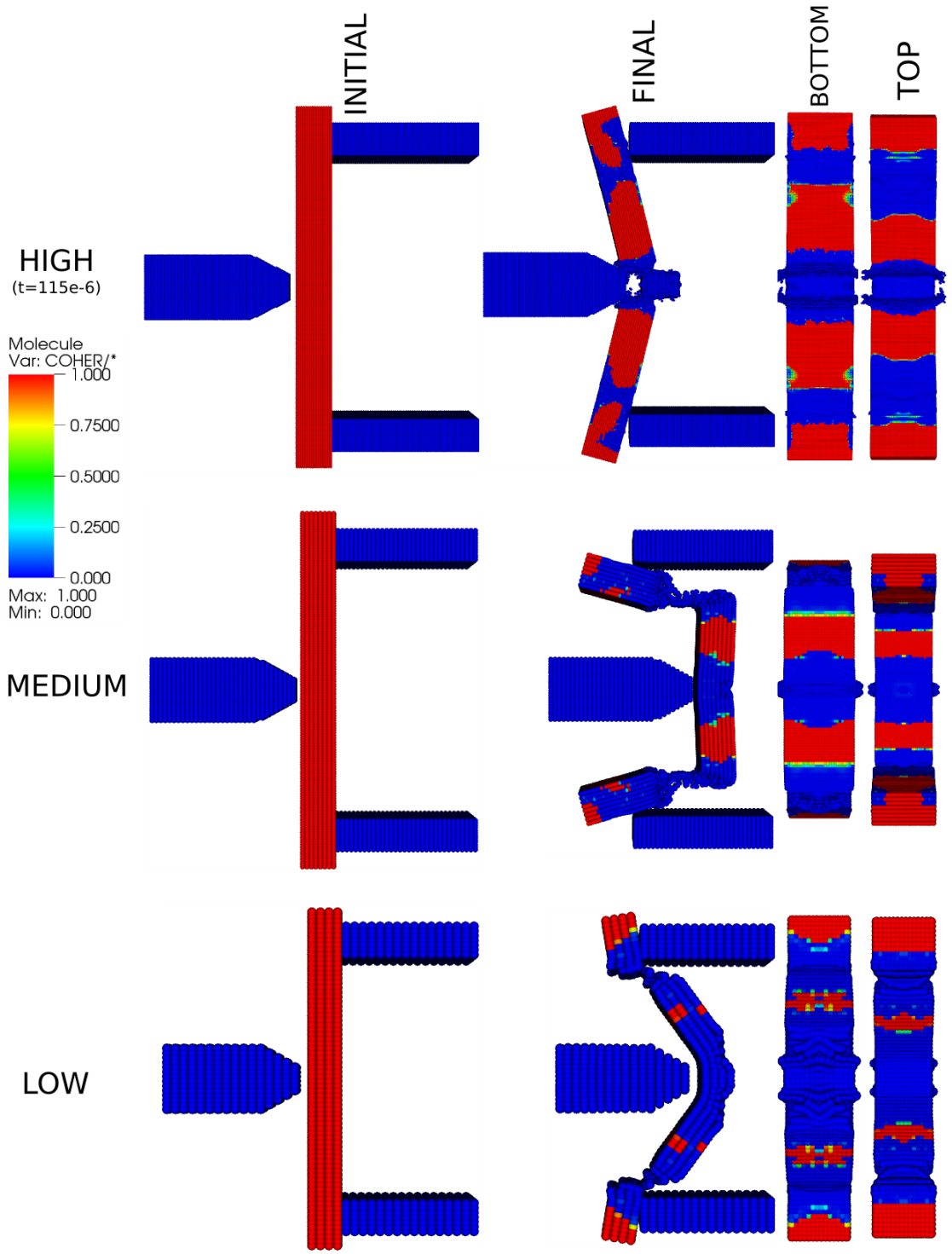


**Figure 6.4**: The Charpy impact problem modeled at three levels of mesh refinement with the original Kayenta fracture model (though with tenuously justified parameters and no material strength variability that has, in other work [2], mitigated mesh dependence). The color in the plot represents `COHER` for the target. The striker and supports are shown with a default value of `COHER` $= 0$ as they are elastic materials and do not soften.

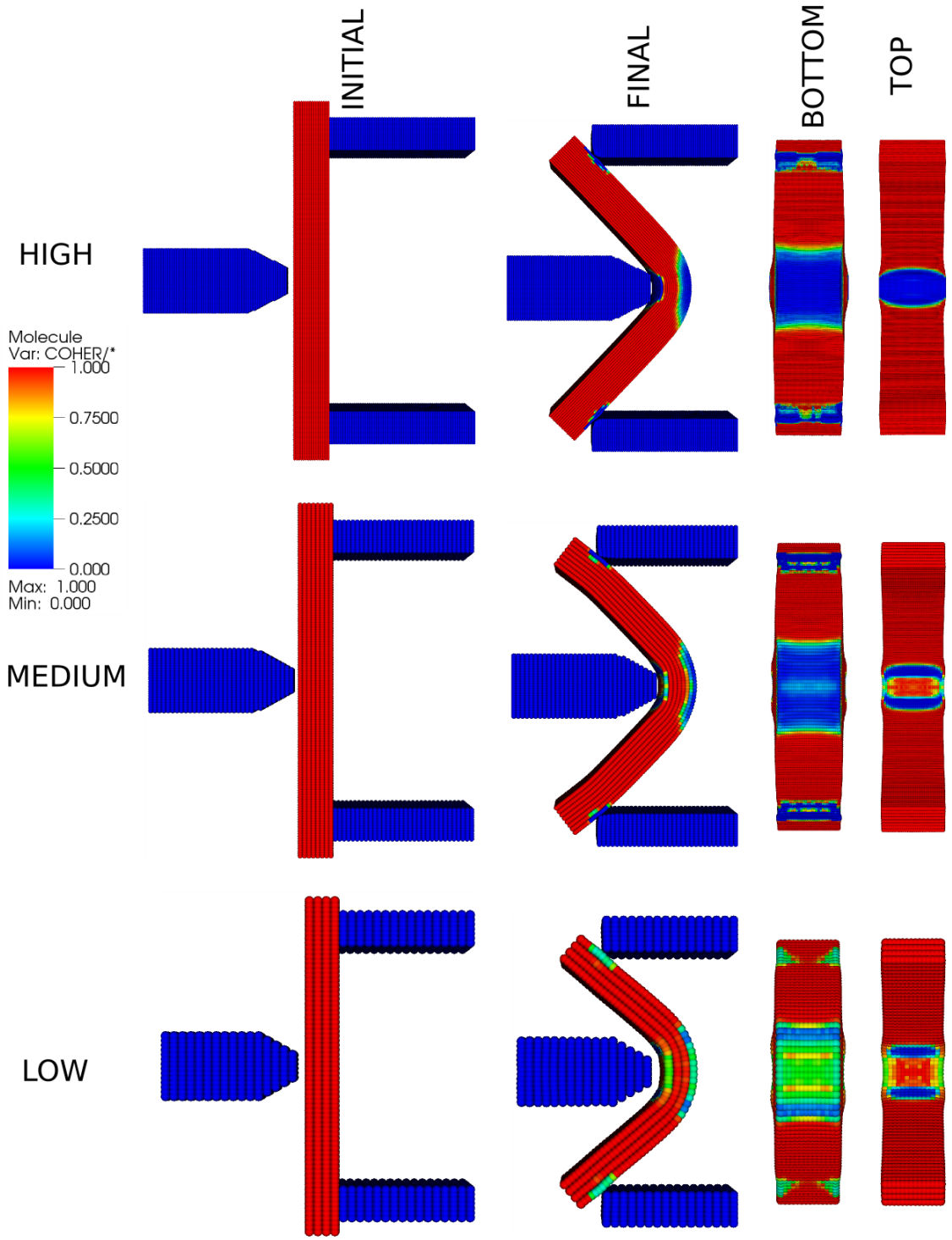


**Figure 6.5**: The Charpy impact problem modeled with the Constant Equivalent-Strain-to-Failure fracture model in Kayenta at three levels of mesh refinement. The color in the plot represents `COHER` for the target. The striker and supports are shown with a default value of `COHER` = 0 as they are elastic materials and do not soften.

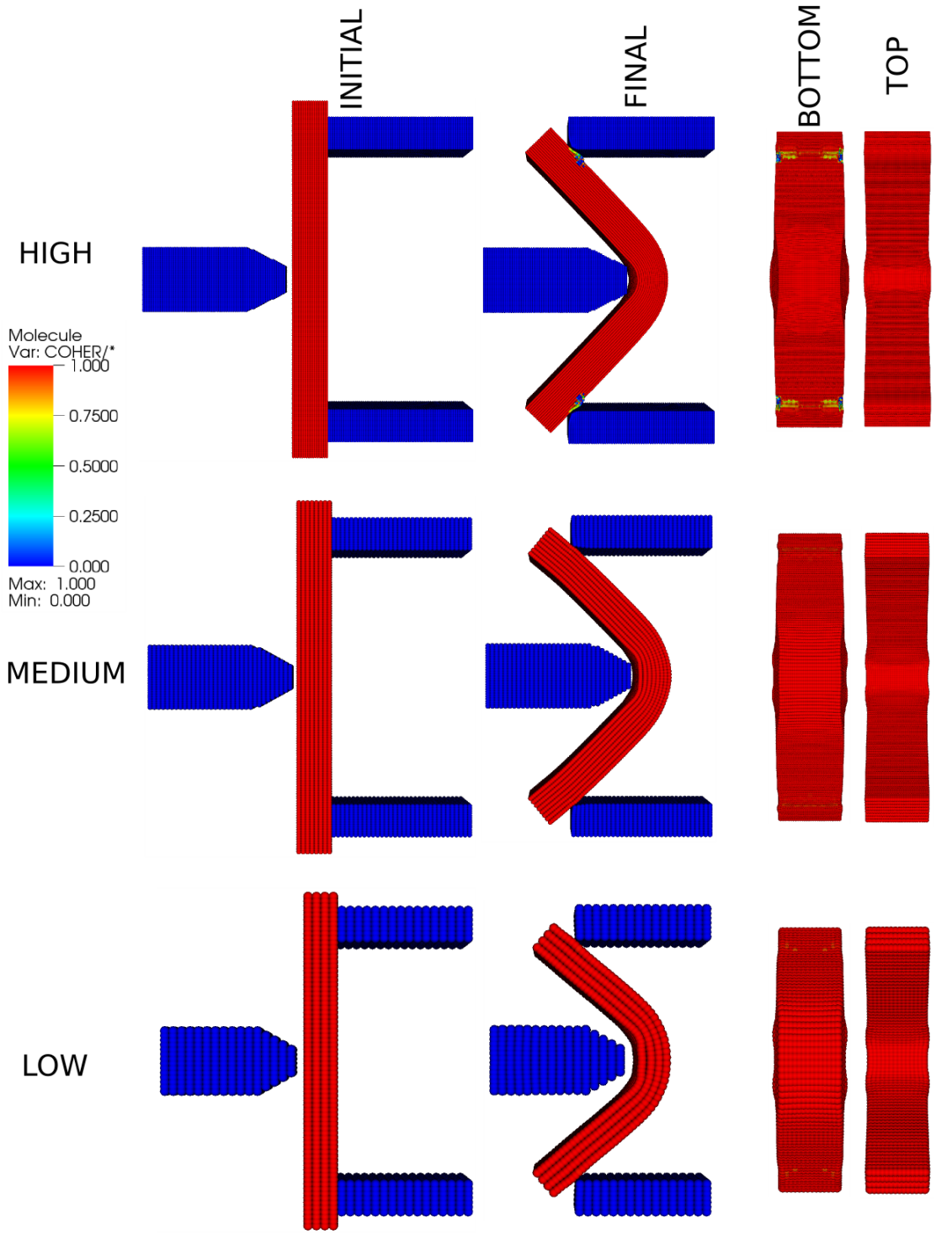


**Figure 6.6**: The Charpy impact problem modeled with the Johnson-Cook fracture model in Kayenta at three levels of mesh refinement. The color in the plot represents `COHER` for the target. The striker and supports are shown with a default value of `COHER` $= 0$ as they are elastic materials and do not soften.

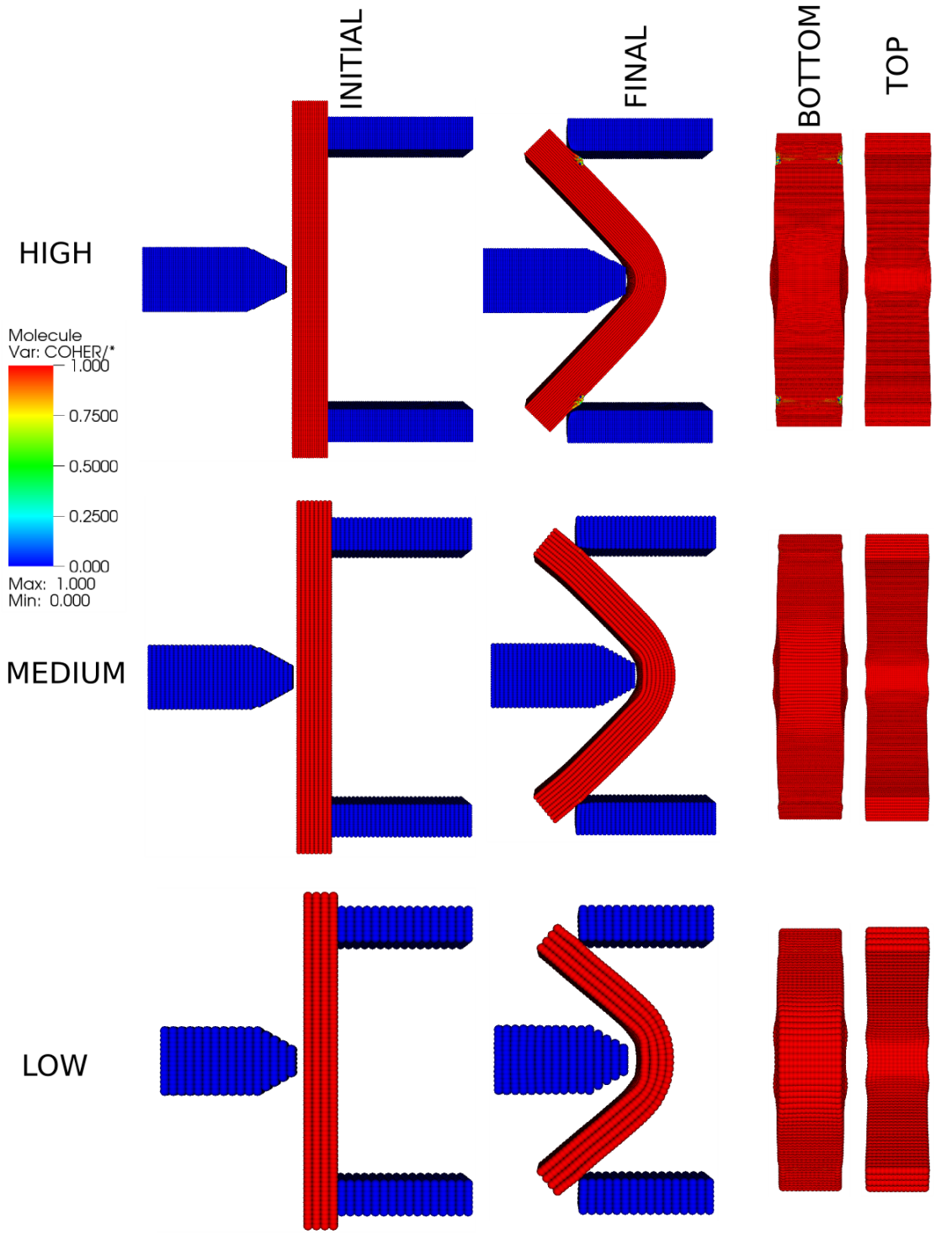


**Figure 6.7**: The Charpy impact problem modeled with the Xue-Wierzbicki fracture model in Kayenta at three levels of mesh refinement. The color in the plot represents `COHER` for the target. The striker and supports are shown with a default value of `COHER` $= 0$ as they are elastic materials and do not soften.

While robustness issues caused the original Kayenta softening model to fail prematurely, the trend of fracture occurring immediately in front of the striker (through the entire thickness) is desirable. There is also significantly more intact material (`COHER` = 1) in the simulations with mesh refinement. It is unclear if mesh- and time-step-refinement alone could cause the model to give accurate results. In fact, similar behavior (namely, a coarse mesh suffering greater damage than a fine mesh) was also reported when using the Kayenta model without statistical variability by Brannon, Wells, et al. [2], and the mesh dependence was virtually eliminated through inclusion of aleatory uncertainty, which has not been included in these simulations but is instead slated to be explored in concurrent research focused exclusively on Charpy validation simulations.

The CESF model shows material failure at the target contact points and opposite the striker. The trend of material failure coalescing towards the center for higher resolutions, as opposed to the strong dual-fracture behavior, is desirable. For the high resolution simulation, nearly all of the material ahead of the striker has failed and is unable to support tensile states. It is expected that a slightly smaller value of the strain-at-failure (which was reported with a very large variance; the mean value was used) would have predicted complete fracture through the specimen. Secondary cracks are not explicitly predicted, but the failed region of the target opposite the striker cannot support tension, thus implying that a secondary crack would be expected in this region. It is expected that inclusion of aleatory uncertainty in these simulations would allow a primary crack to be modeled explicitly.

For the parameters used, both the JC and XW fracture models lacked predictiveness of the fracture patterns actually observed in the experiments. In both sets of simulations, damage occurs only in the high resolution simulations and only at the location of the supports but not at the impact location. It was hypothesized that this lack of fracture might be attributed to the conservative values of the parameters (corresponding to large failure strain) selected for the JC fracture model. The XW parameters share this potential shortcoming since they were derived from the JC parameters. Figure 6.8 demonstrates the discrepancy between the predicted strain-to-failure for the steel paramterizations. It is shocking that the CESF model predicts a failure strain significantly lower than either the Johnson-Cook or Xue-Wierzbicki fracture model. It is not surprising then that there was little to no softening for the simulations using the JC and XW fracture models while significant softening occurred in the simulation using the CESF model. As all these models were parameterized using freely available parameter sets, this underscores the wide variance

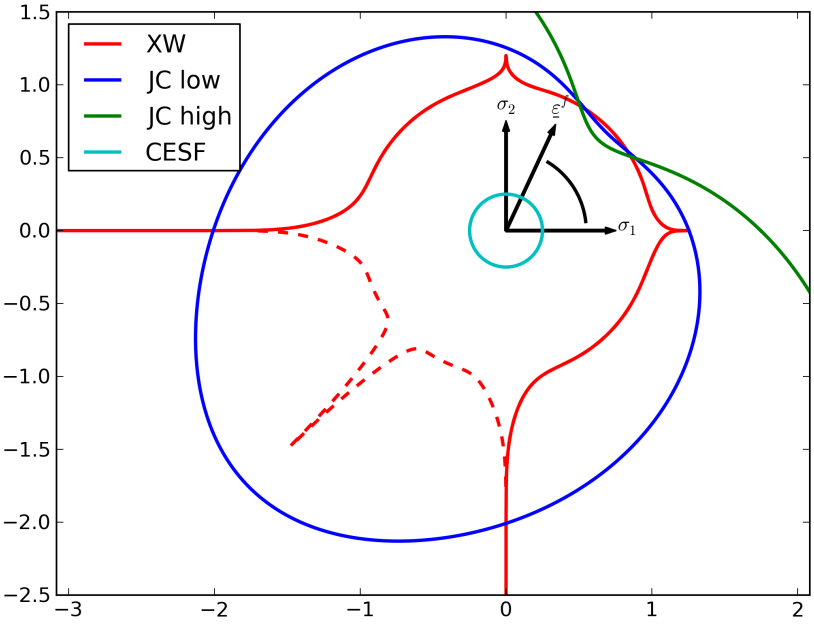


**Figure 6.8**: A polar plot representing equivalent strain-to-failure for plane stress states for models representing 4340 steel. The radius of the polar plot represents the strain-to-failure while the angle defines the ratio of the two nonzero stresses (e.g. 45° corresponds to biaxial tension, 180° and 270° correspond to uniaxial compression). Notice that the CESF model predicts fracture at a much lower strain than the other models. The model "JC low" represents the parameters used in the validation simulation while "JC high" represents the parameters originally published by Johnson and Cook [3]. All other model parameters are listed in Table 6.1. The XW model was parameterized to fit the "JC low" model and does not allow fracture when $\eta \leq -1/3$ (the dotted line denotes the fracture-free region).

in parameter sets that should describe the same material.

In summary, a total of 12 simulations have been presented in this section illustrating the effect of fracture models and mesh resolution on unnotched Charpy impact simulations using otherwise identical models, all implemented in Kayenta to ensure a fair comparison in a common constitutive model framework. Of these, one fracture model (original Kayenta time-based theory) predicted excessive failure and nonconvergence with mesh refinement, and two models (JC and XW) predicted virtually no material damage. Only the simplest of these models (CESF) predicted moderately realistic failure patterns and relatively little mesh dependence. Clearly, model parameterization should be a primary focus of continued research since these simulations alone are not sufficient to rule out the models themselves.

# CHAPTER 7

# SUMMARY AND FUTURE WORK

This research has explored the intricacies of material softening in Kayenta and the possible ramifications of different implementations of the fracture framework. While the end-goal was constant, the method of implementation was undefined, giving broad freedom to explore possible variants. The search for a suitable mechanism for implementing a strain-to-failure framework uncovered several promising projects that could build upon the softening framework. Many of the benefits of this research are currently in use by local researchers and will be disseminated broadly in the next release of Kayenta. As stated in Chapter 6, there is currently an effort underway to rigorously evaluate these fracture models in an unnotched Charpy impact problem.

## 7.1 Future Work

### 7.1.1 Account for Element Size Variability

The original Kayenta framework takes a constant, user-defined value for `TFAIL` that is the same for every element initialized with that material. As the size of the elements might vary, it is no longer reasonable to assume that the time-to-failure should be the same for all elements. Alegra [38] has solved this issue by scaling `TFAIL` for individual elements based on element volume. This causes smaller elements to fail faster than larger elements, giving an ensemble damage velocity that is constant.

The same approach may be applicable to a strain-to-failure model that is based in time-to-failure. However, the current fracture framework gathers no information from the (possibly volume-scaled) `TFAIL` that the user might supply or the host code might compute.

Another broadly accepted method for including scale effects and mitigating mesh sensitivities is nonlocal theory. A natural extension of this work would be to apply the integral-based nonlocal plasticity theory recently implemented in Uintah [41] for this class of problem.

### 7.1.2 Account for Aleatory Uncertainty in Material Properties

The aforementioned scaling accounts for mesh resolution but not for variability in material properties. Another improvement would be adding variability in the strain at failure to cause elements to fail at different times when under homogeneous loading, which has been reported to yield more realistic fracture patterns in some applications [2, 31].

### 7.1.3 Strain-to-Failure with Arresting Coherence

The following research option is a strain analog to the Tresca or Maximum Principal Stress failure criteria for more complex limit surface geometries. While the three models implemented into Kayenta all accumulate damage, there are some potential benefits to having a failure criterion that does not accumulate damage (is path-independent). This suggestion is essentially a proposal to remove the summation symbol from Eq. 4.2 and to have the material lose strength (`COHER` decreases) when $\mathcal{D} = \underline{\varepsilon}/\underline{\varepsilon}^f \geq 1$ and to maintain the current strength when $\mathcal{D} < 1$ (`COHER` stays constant).

When the shear limit surface collapses and decreases the maximum magnitude of $\underline{\sigma}$, the magnitude of stress triaxiality $\eta$ increases (Eq. 2.12). For a Johnson-Cook fracture-type model that has exponential growth in $\underline{\varepsilon}^f$ for increasingly hydrostatically compressive stresses, small increases in the magnitude of $\eta$ can have large increases in $\underline{\varepsilon}^f$, causing the ratio of $\underline{\varepsilon}$ to $\underline{\varepsilon}^f$ to become less than unity and halt the process of softening. This would allow the softening process to converge to states of partial damage and to maintain fractional strength.

This behavior would be especially well-suited for modeling ceramics to represent a material that is neither fully intact nor fully rubblized. For all the implementations currently in Kayenta, when fracture initiates, it will rarely converge to a nonzero value of `COHER`.

### 7.1.4 Interpolated Fracture Models

For low-rate problems, damage velocity is slower than for high-rate problems. Experimental evidence shows that the damage velocity is not linear with respect to loading rate. The fracture velocity increases and asymptotes to the longitudinal wave speed as loading rate increases [37].

Currently, Kayenta can mimic the Johnson-Holmquist models that are generally used for high strain rate applications. On the other extreme, copious experimental evidence [32, 4, 42] supports simple strain-to-failure models for low strain rate applications (especially

for ductile materials). With these models cast in different physical dimensions (time and strain), it would be very difficult to interpolate between them in any meaningful manner to get a hybrid model that could span the range of possible loading scenarios.

The switch to using time as the primary state variable for determining failure in strain-to-failure models unifies these methods into a common dimension and allows an interpolation to be performed between the high-rate models and the low-rate models. While interpolation would yield an educated guess about material response for areas where test data are lacking, it does have some limitations. Naturally, the question arises as to what variable to use as the dependent variable for the interpolation. As we have been differentiating the classes of damage models by strain rate, it would be expected that strain rate could be used as the dependent variable. However, a major drawback to using strain rate is that generally high strain rate problems only sustain that magnitude of strain rate for a small fraction of a second. This situation highlights some issues similar to those encountered in viscoplasticity theory. Specifically, the strength of a material appears to be a function of strain rate provided that strain rate is constant. This poses an issue as high strain rate events tend to only maintain that rate for a short duration. For transient loading, viscoplastic theory treats the strength as a functional of the strain rate governed by a characteristic material response time [43].

These issues highlight some of the difficulty in implementing a dynamically adaptive fracture model. Nevertheless, the framework is in place in Kayenta to allow easy inclusion of this ability once the best dependent variable can be determined for enabling a transition between low-rate and high-rate fracture models.

## 7.2 Summary

This research has addressed the need to have a generalized plasticity model that is capable of approximating a variety of softening models. The deliverables of this research are:

- **Literature Review** This in-depth review will help others to evaluate some of the more recent fracture models being proposed and to choose fracture models in an informed manner, knowing the strengths and limitations of the the models surveyed.
- **Strain-to-Failure Framework** This framework has been written to allow easy implementation of other damage models that use linear accumulation of damage. Also, the original softening framework has not been altered.
- **Three Strain-to-Failure Models** The implementation of the constant equivalent-strain-to-failure model, the Johnson-Cook fracture model, and the Xue-Wierzbicki

fracture model, has enabled Kayenta to approximate five different softening models, selected through input parameters. This allows greater flexibility and helps researchers to quickly choose the models that they deem applicable for a given situation.

- **Verification** The models and framework have been extensively verified and have been found to behave as expected. As the initial verification is complete, benchmarks are in place that regularly exercise this functionality. With the burden of framework verification removed, future developers can focus on implementing new fracture models and peforming verification of their own work.
- **Validation** This research does not seek to quantify the agreement between the three strain-to-failure fracture models and the experiments; it does demonstrate the utility of the framework and the effects that can be observed.

These deliverables represent a step forward in the development and inclusion of fracture models into Kayenta as a generalized softening framework, as well as a generalized plasticity framework. The fracture models included have added stress dependence on the softening response, which is anticipated to lead to more predictive results.

# APPENDIX

# SOURCE CODE EXCERPTS

The following is the FORTRAN77 routine that dynamically computes the value of `TFAIL` to reproduce a strain-to-failure behavior without changing the native softening implementation in Kayenta.

There are sections that are noncritical (such as host-code specific #IFDEF statements) that have been replaced by [[ redacted]] .

## A.1 Inputs and Constants

This section shows the function calling arguments, a small description of the inputs, and also defines the constants used. The function EXPS() is not a regularly-defined function in FORTRAN 77, but is simply a safe version of the EXP() function to account for overflow/underflow problems by using MIN() and MAX() on the input to ensure that the output can be represented by all compilers.

```
      SUBROUTINE KMM_UPDFRC(SV,SIG,DE,EQDOT)
C**********************************************************************
C     PURPOSE: Reproduce strain-to-failure damage behavior without
C              changing the native softening framework already present
C              in Kayenta. This routine can easily be expanded to
C              include any linear accumulation, strain-to-failure damage
C              model.
C
C input
C -----
C     SV()  - The state variable array
C     SIG() - The stress array
C     DE()  - The strain increment array (reflects subcycling)
```

```
C     EQDOT - The current strain rate
C
C output
C -----
C     SV(KTFAIL)
C
C  AUTHORS
C  mss: Scot Swan : Creator
C
C  MODIFICATION HISTORY
C  yymmdd|usrname|what was done
C  ------ --- -------------
C  111212|mss|Finishing polish on the routine.
C
C*********************************************************************
[[redacted]]
      PARAMETER (PZERO=0.0D0,PONE=1.D0,PTWO=2.D0,PTHREE=3.D0,BIG=1.D99)
      PARAMETER (P1P5=1.5D0)
      PARAMETER (PTHIRD=0.33333333333333333333333333333333333333333333D0)
      PARAMETER (PSIXTH=0.16666666666666666666666666666666666666666666D0)
      PARAMETER (PTHRTNP5=13.5D0)
      PARAMETER (ROOT2=0.14142135623730950488016887242096980785696718D1)
      PARAMETER (TOOR2=0.70710678118654752440084436210484903928483593D0)
      PARAMETER (ROOT3=0.17320508075688772935274463415058723669428052D1)
      PARAMETER (TOOR3=0.57735026918962573245977067410922532560270479D0)
C.....................................................................passed
[[redacted]]
      DIMENSION SV(*), SIG(*), DE(*)
C.....................................................................functions
C.....................................................................external
#ifdef IMPLNONE
      DOUBLE PRECISION EXPS
#endif
C.....................................................local scalars
```

```
#ifdef IMPLNONE
      DOUBLE PRECISION DUM, EQDE, SIGMEAN, SIGEQUIV, ETA, XI,  FUNC
#endif
```

## A.2 Preprocessing

In this section, we see (in order of use)

- **Eq. 2.15** This is used to compute the strain increment which updates the damage state variable. This is then used to increment the accumulated strain state variable (solely used for verification purposes).
- **Eq. 2.10** Used to compute the mean stress, $\sigma_m$.
- **Eq. 2.11** Used to compute the equivalent stress, $\underline{\sigma}$.
- **Eq. 2.12** Used to compute the equivalent stress. Notice the checks for hydrostatic stress states and the default of $\eta = 0$ when $\sigma_m = \underline{\sigma} = 0$.
- **Eq. 2.13** Used to compute the deviatoric state parameter, $\xi$, with a default value of zero for a zero-stress state. Also, ensure that $-1 \leq \xi \leq +1$.

```
CCCCCCCCCCCCCCCCCCCCCCCCCCCCCCCCCCCCCCCCCCCCCCCCCCCCCCCCCCCCCCC KMM_UPDFRC
C------------------------------------------- CALCULATE STRAIN INCREMENT
      EQDE = DE(1)*DE(1) + DE(2)*DE(2) + DE(3)*DE(3)
     &     + PTWO*(DE(4)*DE(4) + DE(5)*DE(5) + DE(6)*DE(6))
      EQDE = ROOT2*TOOR3*SQRT(EQDE)
      SV(KACCSTRAIN)=SV(KACCSTRAIN)+EQDE
C------------------------------------------------------------ EARLY EXIT
C     If, for some reason, this routine is being called when STRNFRC
C     (strain-controlled fracture) not wanted or when TGROW has already
C     surpassed TFAIL (fracture has already occurred), exit.
      IF( .NOT. STRNFRC .OR. SV(KTGROW).GT.SV(KTFAIL) ) RETURN
C
C------------------------------------------------------------- SET INPUTS
C     Set FUNC and DUM to some preset because the compiler complains
C     about them possibly being used uninitialized.
      FUNC = PONE
      DUM  = PONE
C------------------------------------------------ COMPUTE STRESS MEASURES
C     Calculate the mean stress.
```

```
      SIGMEAN = (SIG(1)+SIG(2)+SIG(3))/PTHREE
C
C     Compute J2 then the von Mises equivalent stress
C                  (SIGEQUIV) = sqrt(3*J2)
      SIGEQUIV = PSIXTH*( (SIG(1)-SIG(2))**PTWO
     &                   +(SIG(2)-SIG(3))**PTWO
     &                   +(SIG(3)-SIG(1))**PTWO)
     &                   + SIG(4)*SIG(4)
     &                   + SIG(5)*SIG(5)
     &                   + SIG(6)*SIG(6)
      SIGEQUIV = SQRT(PTHREE*SIGEQUIV)
C
C     Compute triaxiality, ETA (dimensionless pressure-stress ratio)
C     and XI (deviatoric state parameter). If SIGEQUIV == 0, we have
C     a purely hydrostatic state. if SIGMEAN == 0 also, triax is zero.
C         Set XI = J3 = det(S) then XI = 27/2*J3/SIGEQUIV**3
      ETA = PZERO
      XI  = PZERO
      IF (SIGEQUIV.NE.PZERO) THEN
          ETA = SIGMEAN/SIGEQUIV
          XI = ((SIG(2)-SIGMEAN)*(SIG(3)-SIGMEAN)-SIG(5)*SIG(5))
     &                                              *(SIG(1)-SIGMEAN)
     &         -(SIG(4)*(SIG(3)-SIGMEAN)-SIG(6)*SIG(5))*SIG(4)
     &         +(SIG(4)*SIG(5)-SIG(6)*(SIG(2)-SIGMEAN))*SIG(6)
          XI  = MIN(PONE,MAX(-PONE,PTHRTNP5*XI/SIGEQUIV**PTHREE))

      ELSE
          IF (SIGMEAN.LT.PZERO) THEN
              ETA = -BIG
          ELSE
              ETA = BIG
          ENDIF
      ENDIF
C
```

## A.3 Framework Documentation

This part of the source documents Eq. 4.2 and clarifies what the framework requires of new models.

```
C---------------------------------------------- FRAMEWORK DOCUMENTATION
C     The following code (to the end of the routine) has been written
C     to be easily expandable to include as many damage models that
C     use the linear accumulation of damage. It assumes that the FDAMAGE
C     parameter starts at zero and proceeds to unity where fracture
C     occurs. The evolution of damage does not correlate to any change
C     in material response until fracture is predicted.
C     So, models that can be written in the form can be used:
C
C                          ----
C                          \      d\epsilon
C                    D =    )    -----------
C                          /       F(...)
C                          ----
C
C     By the end of each block of code, the variable FUNC must be
C     set to the value of the function F(...) for the given material
C     state.
C
C     The integer-value of the user input SOFTENING is used to
C     determine the fracture model. For legacy reasons, SOFTENING=2 is
C     reserved for the original softening implementation, so numbering
C     here begins at 3.
C
C         NSOFT == 3   Constant Strain at Fracture
C         NSOFT == 4   Johnson Cook Fracture[1]
C         NSOFT == 5   Xue-Wierzbicki Fracture[2]
C
```

## A.4 Compute Model-Specific Equivalent Strain at Failure

This section shows how the three fracture models have been implemented into the fracture framework. The following equations are used:

- **Eq. 4.3** Equation for the equivalent plastic strain at failure, $\underline{\varepsilon}^f$, for the constant-strain-to-failure model.
- **Eq. 4.4** Equation for the equivalent plastic strain at failure, $\underline{\varepsilon}^f$, for the Johnson-Cook fracture model. Although Johnson [3] specifically states that his model is only valid for $\eta \leq 1.5$, the code reflects the implementation of this model in Uintah [16] and enforces the constraint of $-1.5 \leq \eta \leq 1.5$.
- **Eq. 4.6** Equation for the equivalent plastic strain at failure, $\underline{\varepsilon}^f$, for the Xue-Wierzbicki fracture model [4]. While the default is to run with the model exactly as is described in the original publication, there is a user input to toggle the use of the fracture cutoff.

```
      IF (NSOFT.EQ.3) THEN
C---------------------------------------------- CONSTANT STRAIN FRACTURE
C         This model is very simple, the equivalent strain at failure
C         function, F(...), is constant. That constant is set by the
C         first failure input (XC1).
          FUNC = XC1
      ELSE IF (NSOFT.EQ.4) THEN
C---------------------------------------------- JOHNSON COOK FRACTURE [1]
C         Inputs
C           XC1 = D1     XC5 = D5
C           XC2 = D2     XC6 = reference strain rate
C           XC3 = D3     XC7 = melt temperature
C           XC4 = D4     XC8 = room temperature

C         Compute the contribution of the stress part
C         ETA is limited to be within -1.5 <= ETA <= 1.5
C         This is a limitation documented in [1].
          FUNC = XC1 + XC2*EXPS(XC3*MAX(-P1P5,MIN(P1P5,ETA)))
C
```

```
C         Compute the strain rate contribution (as it is coded
C         in Uintah as of December 2011).
          IF (EQDOT.LT.PONE) THEN
              FUNC = FUNC*(1.0+EQDOT)**XC4
          ELSE
              FUNC = FUNC*(PONE + XC4*LOG(EQDOT/XC6))
          ENDIF
C
C         Compute the temperature contribution to finish off the
C         equivalent strain at failure for the loading conditions.
          FUNC = FUNC*(PONE + XC5*(SV(KTMPR)-XC8)/(XC7-XC8))
C
      ELSE IF (NSOFT.EQ.5) THEN
C---------------------------------------- XUE-WIERZBICKI FRACTURE [2]
C         As it is written in [2], we are using the following user
C         inputs as Wierzbicki variables:
C                 XC1 = C1     XC3 = C3     XC5 = N
C                 XC2 = C2     XC4 = C4     XC6 = toggle cutoff
C
C          Implement the Bao-Wierzbicki fracture cutoff if XC6 == 0
C          (the default) and triaxiality is <= -1/3, otherwise proceed
C          as usual.
           IF (XC6.EQ.PZERO.AND.ETA.LE.-PTHIRD) THEN
               FUNC = BIG
           ELSE
C                        This computes the even integer nearest
C                            to the value of 1/N.
C                              ____________/\_____________
C                             /                           \
               DUM = PONE-XI**(PTWO*DNINT(PONE/(PTWO*XC5)))
               DUM = DUM**XC5
C
C              Set FUNC to the equivalent strain at failure function
C              For the loading conditions.
```

```
                FUNC = XC1*EXPS(-XC2*ETA)*(PONE-DUM)
     &                + XC3*EXPS(-XC4*ETA)*DUM
          ENDIF
       ENDIF
C
```

## A.5 Update Damage

Here, we have the application of Eq. 4.2 to update the damage value and make sure that $0 \leq \mathcal{D} \leq +1$.

```
C------------------------------------------------------------ UPDATE DAMAGE
C     Add to the damage SV. All models above give an equivalent
C     strain at failure and we add the fractional increase for
C     the strain increment. Ensure that Damage <= one.
      DUM = EQDE/FUNC
      IF (DUM.GT.PZERO) SV(KFDAMAGE) = SV(KFDAMAGE) + DUM
      IF (SV(KFDAMAGE).GE.PONE) SV(KFDAMAGE) = PONE
C
```

## A.6 Compute and Set TFAIL

The following section evaluates Eq. 4.8 and performs several checks on the value of TFAIL before setting the value in the state variable array. Also, this block of code contains the end of the routine with the small bibliography for citations used in the comments.

```
C------------------------------------------------------------ COMPUTE TFAIL
C     Compute the remaining strain to fracture with the assumption
C     that the loading will continue unchanged. FUNC is repurposed
C     to now contain the remaining strain to failure (up to this
C     point FUNC has been the strain-at-failure value for the
C     loading state).
      FUNC = (PONE-SV(KFDAMAGE))*FUNC
C
C     Compute the tentative value of TFAIL. Ensure that if the strain
C     rate is zero that it will give a computationally meaningful
```

```
C     result. The tentative value of TFAIL is simply TGROW (the current
C     amount of time that the stress state has been at the limit
C     surface) plus how much time it would take, at the current strain
C     rate, to attain a damage value of one.
      IF (EQDOT.LE.PZERO) THEN
          DUM = TGROW + PONE
      ELSE
          DUM = ROOT3*TOOR2*FUNC/EQDOT + TGROW
      ENDIF
C
C     Finally, do a check for a realistic result (non-negative values).
C     Then, load the new TFAIL value into the state variable array.
      IF (DUM.LT.PZERO) THEN
          SV(KTFAIL) = PZERO
      ELSE
          SV(KTFAIL) = DUM
      ENDIF
C-----------------------------------------------------------------------
C                              BIBLIOGRAPHY
C     [1] Gordon R. Johnson and William H. Cook. Fracture
C         characteristics of three metals subjected to various
C         strains, strain rates, temperatures and pressures.
C         Engineering Fracture Mechanics, 21(1):31-48, 1985
C     [2] Tomasz Wierzbicki, Yingbin Bao, Young-Woong Lee, and
C         Yuanli Bai. Calibration and evaluation of seven fracture
C         models. International Journal of Mechanical Sciences,
C         47(4-5):719  743, 2005.
C-----------------------------------------------------------------------
      RETURN
      END
```

# REFERENCES


[1] Brannon, R., Fossum, A., and Strack, O., 2009. "Kayenta: theory and user's guide," Tech. Rep. SAND2009-2282, USDOE, Mar.

[2] Brannon, R., Wells, J., and Strack, O., 2007. "Validating theories for brittle damage," Metallurgical and Materials Transactions A, **38**, pp. 2861–2868.

[3] Johnson, G., and Cook, W., 1985. "Fracture characteristics of three metals subjected to various strains, strain rates, temperatures and pressures," Engineering Fracture Mechanics, **21**(1), pp. 31 – 48.

[4] Wierzbicki, T., Bao, Y., Lee, Y., and Bai, Y., 2005. "Calibration and evaluation of seven fracture models," International Journal of Mechanical Sciences, **47**(4-5), pp. 719 – 743.

[5] Timmel, M., Kolling, S., Osterrieder, P., and Bois, P. D., 2007. "A finite element model for impact simulation with laminated glass," International Journal of Impact Engineering, **34**, pp. 1465–1478.

[6] Teng, X., Wierzbicki, T., Hiermaier, S., and Rohr, I., 2005. "Numerical prediction of fracture in the taylor test," International Journal of Solids and Structures, **42**(9-10), pp. 2929 – 2948.

[7] Bishop, J., 2008. "Notes on the article "calibration and evaluation of seven fracture models," by Wierzbicki et al.," Dec.

[8] Xue, L., 2007. "Damage accumulation and fracture initiation in uncracked ductile solids subject to triaxial loading," International Journal of Solids and Structures, **44**(16), pp. 5163 – 5181.

[9] Bao, Y., and Wierzbicki, T., 2004. "On fracture locus in the equivalent strain and stress triaxiality space," International Journal of Mechanical Sciences, **46**(1), pp. 81 – 98.

[10] Reddy, J., 2008. *An Introduction to Continuum Mechanics with Applications*, 1st ed. Cambridge University Press.

[11] Bretscher, O., 2004. *Linear Algebra with Applications*, 3rd ed. Prentice Hall.

[12] Lode, W., 1926. "Versuche ber den einflu der mittleren hauptspannung auf das flieen der metalle eisen, kupfer und nickel," Zeitschrift fr Physik A Hadrons and Nuclei, **36**, pp. 913–939.

[13] Bai, Y., and Wierzbicki, T., 2007. "A new model of metal plasticity and fracture with pressure and lode dependence," International Journal of Plasticity, **24**(6), pp. 1071 – 1096.

[14] Seth, B., 1961. "Generalized strain measure with applications to physical problems," Tech. rep., Wisconsin University - Madison Mathematics Research Center, Jul.

[15] Hallquist, J., 2006. *LS-DYNA Theory Manual* Livermore Software Technology Corporation, Mar.

[16] Guilkey, J., Harman, T., and Luitjens, J., 2011. *Uintah User Guide*, 1.3 ed. Center for the Simulation of Accidental Fires and Explosions, Sep.

[17] Teng, X., and Wierzbicki, T., 2006. "Evaluation of six fracture models in high velocity perforation," Engineering Fracture Mechanics, **73**(12), pp. 1653 – 1678.

[18] Driemeier, L., Brunig, M., Micheli, G., and Alves, M., 2010. "Experiments on stress-triaxiality dependence of material behavior of aluminum alloys," Mechanics of Materials, **42**(2), pp. 207 – 217.

[19] Johnson, G., and Cook, W., 1983. "A constitutive model and data for metals subjected to large strains, high strain rates and high temperatures," In Proc. of the 7th International Symposium on Ballistics, The Netherlands, pp. 541–547.

[20] Wilkins, M., Streit, R., and Reaugh, J., 1980. "Cumulative-strain-damage model of ductile fracture: simulation and prediction of engineering fracture tests," Tech. rep., Lawrence Livermore National Laboratory.

[21] Mae, H., Teng, X., Bai, Y., and Wierzbicki, T., 2007. "Calibration of ductile fracture properties of a cast aluminum alloy," Materials Science and Engineering: A, **459**(1-2), pp. 156 – 166.

[22] Mortara, G., 2009. "A hierarchical single yield surface for frictional materials," Computers and Geotechnics, **36**(6), pp. 960 – 967.

[23] Bai, Y., and Wierzbicki, T., 2010. "Application of extended mohr-coulomb criterion to ductile fracture," International Journal of Fracture, **161**(1), pp. 1–20.

[24] Castellanos, C., 2010. "Sensitivity analysis of the johnson-cook plasticity model for hypervelocity impacts: a hydro-code study," Master's thesis, The University of Texas at El Paso, El Paso, Texas.

[25] Coppola, T., Cortese, L., and Folgarait, P., 2009. "The effect of stress invariants on ductile fracture limit in steels," Engineering Fracture Mechanics, **76**(9), pp. 1288 – 1302.

[26] Mirone, G., and Corallo, D., 2010. "A local viewpoint for evaluating the influence of stress triaxiality and lode angle on ductile failure and hardening," International Journal of Plasticity, **26**(3), pp. 348 – 371.

[27] Georgiadis, K., Potts, D. M., and Zdravkovic, L., 2004. "Modelling the shear strength of soils in the general stress space," Computers and Geotechnics, **31**(5), pp. 357 – 364.

[28] Mogi, K., 1971. "Fracture and flow of rocks under high triaxial compression," *Journal of Geophysical Research,* **76**(5), Feb., pp. 1255–1269.

[29] Hollomon, J., 1945. "Tensile deformation," *Metals Technology*, Jun.

[30] Xiao, X., Zhang, W., Wei, G., and Mu, Z., 2010. "Effect of projectile hardness on deformation and fracture behavior in the taylor impact test," Materials and Design, **31**(10), pp. 4913 – 4920.

[31] Brannon, R., and Strack, O., 2006. "Theory and results for incorporating aleatory uncertainty and scale effects in damage models for failure and fragmentation," Oct.

[32] Barsoum, I., and Faleskog, J., 2007. "Rupture mechanisms in combined tension and shear experiments," International Journal of Solids and Structures, **44**(6), pp. 1768 – 1786.

[33] Barsoum, I., and Faleskog, J., 2011. "Micromechanical analysis on the influence of the lode parameter on void growth and coalescence," International Journal of Solids and Structures, **48**(6), pp. 925 – 938.

[34] Johnson, G., and Holmquist, T., 1994. "An improved computational constitutive model for brittle materials," AIP Conference Proceedings, **309**(1), pp. 981–984.

[35] Fuller, T., and Swan, M., 2011. "Payette: an object-oriented material model driver (model developer and user's guide)," This software is research code developed at the University of Utah in collaboration with Sandia National Laboratories., December.

[36] Brannon, R., Burghardt, J., Bauer, S., and Bronowski, D., 2009. "Experimental assessment of unvalidated assumptions in classical plasticity theory," Tech. Rep. SAND2009-0351, Sandia National Laboratories, Jan.

[37] Senf, H., Strassburger, E., and Rothenhausler, H., 1994. "Stress wave induced damage and fracture in impacted glasses," Journal De Physique Iv, **4**(9), pp. 741–746.

[38] Carroll, S. K., and Drake, R. R., 2002. "Alegra: Version 4.6," Tech. Rep. SAND2002-2775, USDOE, Oct.

[39] Crawford, D., Bell, R., Brundage, A., and Hertel, E., 2010. "CTH user's manual and input instructions," Feb.

[40] Callister, W., 2007. *Material Science and Engineering: An Introduction*, 7th ed. John Wiley and Sons, Inc.

[41] Burghardt, J., 2011. "Nonlocal plasticity, instability, and well-posedness of the elastic-plastic initial-boundary value problem," PhD thesis, The University of Utah.

[42] Bai, Y., Teng, X., and Wierzbicki, T., 2009. "On the application of stress triaxiality formula for plane strain fracture testing," Journal of Engineering Materials and Technology, **131**(2).

[43] Reiner, M., 1964. "The deborah number," Physics Today, **17**(1), pp. 62–62.